

Probing generalized parton distributions with electroproduction of lepton pairs off the nucleon

A.V. Belitsky^a, D. Müller^b

*^aDepartment of Physics
University of Maryland at College Park
College Park, MD 20742-4111, USA*

*^bFachbereich Physik, Universität Wuppertal
D-42097 Wuppertal, Germany*

Abstract

We evaluate the differential cross section for the electroproduction of lepton pairs off a polarized nucleon target in the generalized Bjorken region to leading power accuracy in hard momentum. We discuss the importance of this process for phenomenology of generalized parton distributions. A special attention is given to the sensitivity of physical observables, i.e., diverse asymmetries, to their dependence on scaling variables that allows to map directly the functional two-dimensional surface of generalized parton distributions.

Keywords: lepton pair production, asymmetries, generalized parton distributions

PACS numbers: 11.10.Hi, 12.38.Bx, 13.60.Fz

1 Introduction

A quantum mechanical system is determined by its wave function. Acquiring the latter from theoretical considerations, like solving the Schrödinger equation, or experimental measurements allows one to predict any physical observable of the system. The bulk of experimentally accessible quantities is sensitive only to the absolute value of the wave function and the phase of the latter is essentially unattainable. To circumvent the difficulty one has to measure correlations of wave functions, — or more generally the density matrix, — where the phase difference of wave functions can be probed. The interference of a test system with a reference source, possessing an a priori known characteristics, serves the purpose of reconstructing the missing phase of the wave function and thus one acquires complete information on the quantum mechanical system in question.

The nucleon represents a relativistic multi-particle quantum system in a bound state whose dynamic is driven by strong interactions. It is the subject of intensive studies for several decades. Recently, it was realized that the most powerful theoretical tools in the analysis of the nucleon structure are one-quark and one-gluon correlations, dubbed the generalized parton distributions (GPDs) [1, 2, 3]. They are analogous to a field-theoretical generalization of the phase-space Wigner quasi-probability function of non-relativistic quantum mechanics [4, 5], — a specific Fourier transform of a density matrix alluded to above. A GPD depends on several kinematical variables and it has to be mapped as a function of all of them in order to predict such a fundamental quantity as the angular momentum of nucleon's constituents, which is given by their second moment [6]

$$\int_{-1}^1 d\xi \xi \left(H_{q,g}(\xi, \eta, \Delta^2) + E_{q,g}(\xi, \eta, \Delta^2) \right) = 2J_{q,g}. \quad (1)$$

There are essentially three experimentally feasible processes that have a clear theoretical understanding and which can be used for direct measurements of GPDs: electroproduction of the photon $eN \rightarrow e'N'\gamma$ which is sensitive to the deeply virtual Compton scattering (DVCS) amplitude [6, 7, 8, 9], photoproduction of a lepton pair $\gamma N \rightarrow \ell\bar{\ell}N'$ [10], and electroproduction of a lepton pair $eN \rightarrow e'N'\ell\bar{\ell}$ [11, 12]. However, among these only the latter provides a setup necessary for an independent measurement of a GPD as a function of both scaling variables ξ and η . The former two reactions cannot entirely serve the purpose of testing the sum rule due to the reality of the final- or initial-state photons, respectively, which leads to the restriction $\xi = \mp\eta$. The last process is the most challenging from the experimental point of view due to small cross sections involved and requires high energy of the beam and high luminosity, on the one hand, and full exclusivity of the final state, on the other.

The process $eN \rightarrow e'N'\ell\bar{\ell}$ will be the subject of our present study, — a generalization to the full complexity of a short preliminary note [11]. The outline of the paper is as follows. After presenting the general structure of the cross section, kinematical variables and addressing the

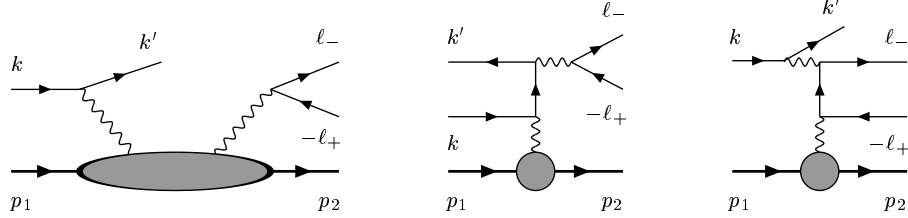


Figure 1: Subprocesses contributing to electroproduction of muon pairs.

issue of reference frames in the next section, we turn to the discussion of the factorization of the process within perturbative QCD in terms of GPDs in section 3. In section 4, we perform the computation of the cross section. We derive first a generating function for the squared of the virtual Compton scattering (VCS) amplitude and its interference with Bethe-Heitler (BH) amplitudes. It has a completely worked out leptonic part while the hadronic piece is expressed in terms of Dirac bilinears involving Compton and electromagnetic form factors. Next, we evaluate the products of bilinears for an unpolarized nucleon target, leaving the longitudinally and transversely polarized options for appendices. In section 5, we give a detailed discussion of diverse asymmetries to be used for extraction of GPDs. Finally, we conclude.

2 Kinematics

The reaction we are dealing with consists of three interfering processes, depicted in Fig. 1 with implied crossed contributions. However, only one of them is sensitive to the one-particle correlations in the nucleon when at least one of the photon virtualities is large compared to a typical hadronic scale. It arises from the virtual Compton scattering amplitude, shown on the left hand side in Fig. 1. The other two amplitudes represent the Bethe-Heitler background. Presently, we discuss the production of a lepton pair of a different flavor compared to the one of the beam, i.e., the muon pair. The consideration of the electroproduction of electron pairs requires the addition of exchange contributions due to identity of the electrons in the final state, i.e., $k' \rightarrow \ell_-$.

2.1 Phase space

The generic form of the cross section of the exclusive electroproduction of lepton pairs off the nucleon, $e(k)N(p_1) \rightarrow e(k')N(p_2)\ell(\ell_-)\bar{\ell}(\ell_+)$, is

$$d\sigma = \frac{1}{4p_1 \cdot k} |\mathcal{T}|^2 d\text{LIPS}_4, \quad (2)$$

where \mathcal{T} is a sum of the amplitude of the virtual Compton scattering and two Bethe-Heitler processes, $\mathcal{T} = \mathcal{T}_{\text{VCS}} + \mathcal{T}_{\text{BH}_1} + \mathcal{T}_{\text{BH}_2}$, displayed in Fig. 1. The four-particle Lorentz invariant phase space

$$d\text{LIPS}_4 = dM_{\ell\bar{\ell}}^2 d\text{LIPS}_3 d\Phi_{\ell\bar{\ell}}, \quad (3)$$

is factorized, by introducing the integration over the invariant mass of the lepton pair $M_{\ell\bar{\ell}}^2$, into Lorentz invariant phase-space factors for the production of a heavy timelike photon off a nucleon

$$d\text{LIPS}_3 = (2\pi)^4 \delta^{(4)}(k + p_1 - k' - p_2 - q_2) \frac{d^4 p_2}{(2\pi)^3} \delta_+(p_2^2 - M_N^2) \frac{d^4 k'}{(2\pi)^3} \delta_+(k'^2) \frac{d^4 q_2}{(2\pi)^3} \delta_+(q_2^2 - M_{\ell\bar{\ell}}^2), \quad (4)$$

and its subsequent decay into a lepton pair

$$d\Phi_{\ell\bar{\ell}} = \frac{d^4 \ell_-}{(2\pi)^3} \delta_+(\ell_-^2 - m_\ell^2) \delta_+((q_2 - \ell_-)^2 - m_\ell^2). \quad (5)$$

A simple calculation gives for them

$$d\text{LIPS}_3 = \frac{dx_B dy d(-\Delta^2) d\phi}{16(2\pi)^4 \sqrt{1 + \varepsilon^2}}, \quad d\Phi_{\ell\bar{\ell}} = \frac{\beta d\Omega_\ell}{8(2\pi)^3}, \quad (6)$$

respectively, where the solid angle of the final state lepton in the $\ell\bar{\ell}$ center-of-mass frame is $d\Omega_\ell = \sin\theta_\ell d\theta_\ell d\varphi_\ell$. Here $\Delta^2 = (p_2 - p_1)^2$ is the momentum transfer in the t -channel and $y = p \cdot q_1 / p \cdot k$ is the incoming lepton energy loss. The conventions for angles are obvious from Fig. 2. Here we introduced the Bjorken variable x_B and we will denote the virtualities of the space- and timelike photons as

$$x_B \equiv \frac{Q^2}{2p_1 \cdot q_1}, \quad q_1^2 \equiv -Q^2, \quad q_2^2 \equiv M_{\ell\bar{\ell}}^2, \quad (7)$$

respectively. The nucleon mass effects are encoded into the variable $\varepsilon \equiv 2x_B M_N / Q$ and the final state lepton velocity in the $\ell\bar{\ell}$ center-of-mass frame reads

$$\beta = \sqrt{1 - 4m_\ell^2 / M_{\ell\bar{\ell}}^2}. \quad (8)$$

Extracting the lepton charge from the amplitudes, one gets for the cross section, expressed in terms of experimentally measurable variables,

$$d\sigma = \frac{\alpha_{\text{em}}^4}{16(2\pi)^3} \frac{x_B y \beta}{Q^2 \sqrt{1 + \varepsilon^2}} \left| \frac{\mathcal{T}}{e^4} \right|^2 dx_B dy d(-\Delta^2) d\phi dM_{\ell\bar{\ell}}^2 d\Omega_\ell. \quad (9)$$

2.2 Reference frames

Let us discuss appropriate reference frames to be used in analytical computations. To have a finite Fourier series of the cross section in terms of the azimuthal angles, we have just introduced

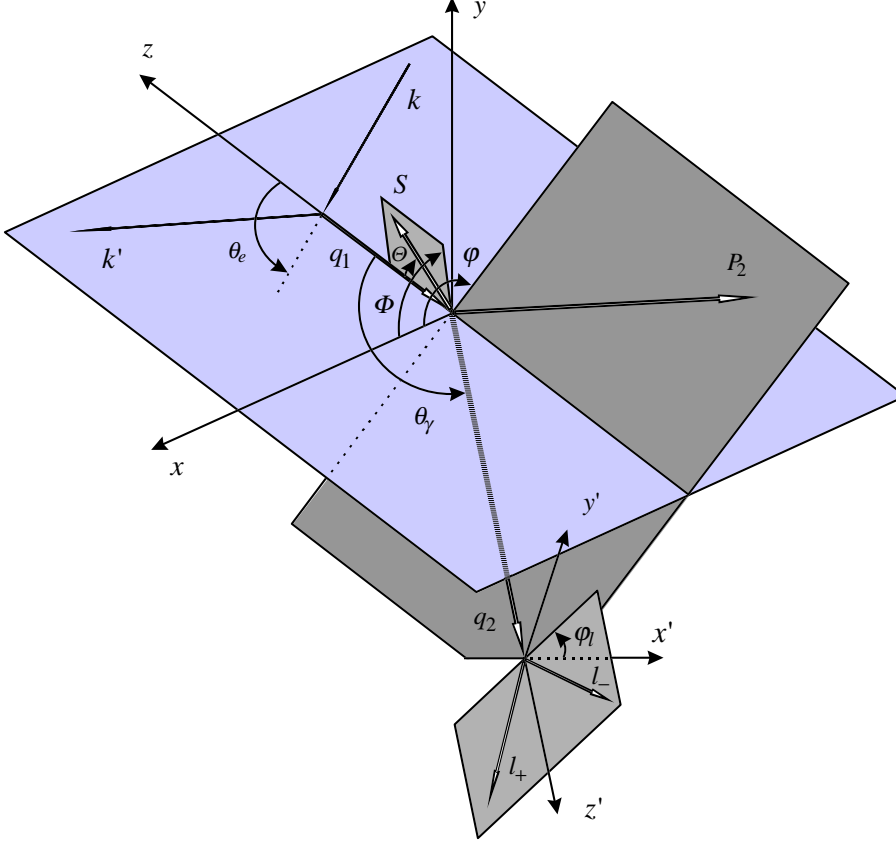


Figure 2: The kinematics of the lepton pair production in elastic electron-nucleon scattering. The coordinate system with the z -axis being counter-aligned to the spacelike virtual photon is termed TRF-I, while the one with z' along the three-momentum of the timelike photon is named TRF-II.

above the target rest frame in which the z -axis is directed in the counter-direction of motion of the spacelike virtual photon, called the target rest frame I (TRF-I), see Fig. 2. In this frame we obviously have

$$p_1 = (M_N, 0, 0, 0), \quad q_1 = (\omega_1, 0, 0, -q_1^z), \quad (10)$$

where

$$\omega_1 = \frac{Q}{\varepsilon}, \quad q_1^z = \frac{Q}{\varepsilon} \sqrt{1 + \varepsilon^2}. \quad (11)$$

For the remaining four-vectors we find:

- The outgoing nucleon momentum $p_2 = (E_2, \vec{p}_2)$ has the components

$$E_2 = M_N - \frac{\Delta^2}{2M_N}, \quad |\vec{p}_2| = \sqrt{-\Delta^2(1 - \Delta^2/(4M_N^2))}, \quad (12)$$

and the scattering angle of the recoiled nucleon is

$$\cos \theta_N = -\frac{\varepsilon^2 (Q^2 + M_{\ell\ell}^2 - \Delta^2) - 2x_B \Delta^2}{4x_B M_N |\vec{p}_2| \sqrt{1 + \varepsilon^2}}. \quad (13)$$

- The incoming electron four-momentum is

$$k = (E, k^x, 0, k^z) = E(1, \sin \theta_e, 0, \cos \theta_e), \quad (14)$$

with

$$E = \frac{\mathcal{Q}}{y\varepsilon}, \quad \cos \theta_e = -\frac{1 + y\varepsilon^2/2}{\sqrt{1 + \varepsilon^2}}, \quad (15)$$

and as a consequence $\sin \theta_e = \varepsilon \sqrt{1 - y - y^2 \varepsilon^2/4} / \sqrt{1 + \varepsilon^2}$.

- The four-vector of the timelike virtual photon reads

$$q_2 = (\omega_2, \vec{v}\omega_2), \quad (16)$$

with

$$\omega_2 = \frac{\mathcal{Q}}{\varepsilon} + \frac{\Delta^2}{2M_N}, \quad v \equiv |\vec{v}| = \sqrt{1 - M_{\ell\ell}^2/\omega_2^2}, \quad (17)$$

To evaluate scalar products which arise in contractions of the leptonic and hadronic tensors, it will be convenient to transform all four-vectors to a frame, termed TRF-II, where the z' -axis is directed along \vec{q}_2 . The latter is achieved by rotating the TRF-I z -axis along the three-velocity \vec{v} of the timelike photon by the scattering angle θ_γ (which lies in the hadron scattering plane),

$$\cos \theta_\gamma = -\frac{\varepsilon (\mathcal{Q}^2 - M_{\ell\ell}^2 + \Delta^2) + 2\mathcal{Q}\omega_2}{2\mathcal{Q}\omega_2 v \sqrt{1 + \varepsilon^2}}. \quad (18)$$

In TRF-II, $q_2 = (\omega_2, 0, 0, \omega_2 v)$, and for the other momenta we get

$$q_1 = (\omega_1, q_1^z \sin \theta_\gamma, 0, -q_1^z \cos \theta_\gamma), \quad (19)$$

and

$$k = E (1, \sin \theta_e \cos \theta_\gamma \cos \varphi_\gamma - \cos \theta_e \sin \theta_\gamma, -\sin \theta_e \sin \varphi_\gamma, \sin \theta_e \sin \theta_\gamma \cos \varphi_\gamma + \cos \theta_e \cos \theta_\gamma), \quad (20)$$

with $\varphi_\gamma = \pi + \phi$. In TRF-II the vector p_1 is unchanged. In these formulas, the sinus of θ_γ is given by

$$\sin \theta_\gamma = \frac{\sqrt{4x_B(1 - x_B) + \varepsilon^2}}{2\mathcal{Q}\omega_2 v \sqrt{1 + \varepsilon^2}} \sqrt{-(\Delta^2 - \Delta_{\min}^2)(\Delta^2 - \Delta_{\max}^2)}, \quad (21)$$

in terms of the maximal and minimal momentum transfer in the t -channel,

$$\Delta_{\min, \max}^2 = -\frac{1}{4x_B(1 - x_B) + \varepsilon^2} \left\{ 2 \left((1 - x_B) \mathcal{Q}^2 - x_B M_{\ell\ell}^2 \right) + \varepsilon^2 (\mathcal{Q}^2 - M_{\ell\ell}^2) \right. \\ \left. \mp 2\sqrt{1 + \varepsilon^2} \sqrt{\left((1 - x_B) \mathcal{Q}^2 - x_B M_{\ell\ell}^2 \right)^2 - \varepsilon^2 \mathcal{Q}^2 M_{\ell\ell}^2} \right\}, \quad (22)$$

with $- (+)$ corresponding to Δ_{\min}^2 (Δ_{\max}^2).

A boost from the timelike photon rest frame to the TRF-II along the direction of motion of the photon with velocity \vec{v} , see Eq. (17), yields

$$\ell_- = \left(\frac{1}{2}\omega_2(1 + v\beta \cos \theta_\ell), \frac{1}{2}M_{\ell\bar{\ell}}\beta \sin \theta_\ell \cos \varphi_\ell, \frac{1}{2}M_{\ell\bar{\ell}}\beta \sin \theta_\ell \sin \varphi_\ell, \frac{1}{2}\omega_2(v + \beta \cos \theta_\ell) \right), \quad (23)$$

where θ_ℓ and φ_ℓ are the solid angles of ℓ_- in the $\ell\bar{\ell}$ center-of-mass frame alluded to above. The vector ℓ_+ is simply deduced by a reflection, $\varphi_\ell \rightarrow \varphi_\ell + \pi$ and $\theta_\ell \rightarrow \pi - \theta_\ell$, from ℓ_- (or equivalently by the substitution $\beta \rightarrow -\beta$).

Using the explicit form of four-vectors in the TRF-II, we can readily compute the invariant products. Namely, the most nontrivial scalar products are

$$\begin{aligned} k \cdot \Delta &= -\frac{1}{2y(1 + \varepsilon^2)} \left\{ \left(\mathcal{Q}^2 + M_{\ell\bar{\ell}}^2 \right) \left(1 - 2K \cos \varphi_\gamma + \frac{y\varepsilon^2}{2} \right) - \Delta^2 \left(1 - x_B(2 - y) + \frac{y\varepsilon^2}{2} \right) \right\}, \quad (24) \\ \ell_- \cdot \Delta &= -\frac{\beta}{4v} \left\{ \left(\mathcal{Q}^2 + M_{\ell\bar{\ell}}^2 \right) \left(\frac{v}{\beta} + \cos \theta_\ell + 2 \frac{\mathcal{Q}M_{\ell\bar{\ell}}}{\mathcal{Q}^2 + x_B\Delta^2} \frac{K \sin \theta_\ell \cos \varphi_\ell}{\sqrt{1 - y - y^2\varepsilon^2/4}} \right) \right. \\ &\quad \left. + \Delta^2 \left(\frac{v}{\beta} + \frac{\mathcal{Q}^2 - 2x_B M_{\ell\bar{\ell}}^2 + x_B\Delta^2}{\mathcal{Q}^2 + x_B\Delta^2} \cos \theta_\ell \right) \right\}. \quad (25) \end{aligned}$$

where

$$K \equiv \frac{1}{2(\mathcal{Q}^2 + M_{\ell\bar{\ell}}^2)} \sqrt{-(1 - y - y^2\varepsilon^2/4)(4x_B(1 - x_B) + \varepsilon^2)(\Delta^2 - \Delta_{\min}^2)(\Delta^2 - \Delta_{\max}^2)}. \quad (26)$$

Eq. (24) reduces to the known expression from Ref. [9] for the real final-state photon $M_{\ell\bar{\ell}} = 0$. Finally, since the expression for $\ell_- \cdot k$ is too complex to be presented here, we will give below its expanded form which is used in all practical calculations. To make the results look symmetric, we introduce the variable

$$\frac{1}{\tilde{y}} \equiv \frac{p_1 \cdot \ell_-}{p_1 \cdot q_2} = \frac{1 + v\beta \cos \theta_\ell}{2} \simeq \frac{1 + \cos \theta_\ell}{2}, \quad (27)$$

which varies in the interval $1 \leq \tilde{y} \leq \infty$.

2.3 Symmetric variables

For our subsequent use, we introduce the symmetric combinations of momenta

$$q = \frac{1}{2}(q_1 + q_2), \quad p = p_1 + p_2, \quad \Delta = p_2 - p_1 = q_1 - q_2, \quad (28)$$

and the invariants built from them

$$q^2 = -Q^2, \quad \xi = \frac{Q^2}{p \cdot q}, \quad \eta = \frac{\Delta \cdot q}{p \cdot q}, \quad (29)$$

with the latter two being the generalized Bjorken and skewness variables, respectively. These can be re-expressed in terms of experimental ones, discussed in the previous section, via the equations:

$$Q^2 = \frac{1}{2} \left(\mathcal{Q}^2 - M_{\ell\ell}^2 + \frac{\Delta^2}{2} \right), \quad (30)$$

for the inverse resolution scales, and

$$\xi = -\eta \frac{\mathcal{Q}^2 - M_{\ell\ell}^2 + \Delta^2/2}{\mathcal{Q}^2 + M_{\ell\ell}^2}, \quad \eta = -\frac{\mathcal{Q}^2 + M_{\ell\ell}^2}{2\mathcal{Q}^2/x_B - \mathcal{Q}^2 - M_{\ell\ell}^2 + \Delta^2}, \quad (31)$$

for the scaling variables. Note that Q^2 and ξ can take both positive ($\mathcal{Q}^2 > M_{\ell\ell}^2$) and negative ($\mathcal{Q}^2 < M_{\ell\ell}^2$) values depending on the relative magnitude of spacelike and timelike photon virtualities, while $\eta < 0$ and $\pm\xi - \eta > 0$. To complete the set of formulas, the inverse transformations read

$$M_{\ell\ell}^2 = -\left(1 + \frac{\eta}{\xi}\right) Q^2 + \frac{\Delta^2}{4}, \quad \mathcal{Q}^2 = \left(1 - \frac{\eta}{\xi}\right) Q^2 - \frac{\Delta^2}{4}, \quad (32)$$

and

$$x_B = \frac{(\xi - \eta)Q^2 - \xi\Delta^2/4}{(1 - \eta)Q^2 - \xi\Delta^2/2}. \quad (33)$$

The bulk of results given in subsequent sections will be presented in the symmetric variables. The following scalar products are needed in course of evaluations. Neglecting the nucleon mass corrections $\sim M_N^2/Q^2$, the above formulas (22) simplify considerably

$$\Delta_{\min}^2 \approx -4M_N^2 \frac{\eta^2}{1 - \eta^2}, \quad \Delta_{\max}^2 \approx -Q^2 \frac{1 - \eta^2}{\xi(1 - \xi)},$$

and the transverse momentum transfer admits the form $\Delta_{\perp}^2 \approx (1 - \eta^2)(\Delta^2 - \Delta_{\min}^2)$. The $1/(p \cdot q)$ -expansion of the scalar products (24), (25), and $\ell_- \cdot k$, keeping the leading and sub-leading terms only, results into expressions

$$k \cdot \Delta \approx \frac{Q^2}{y} \frac{\eta}{\xi} (1 - 2K \cos \varphi_\gamma), \quad (34)$$

$$\ell_- \cdot \Delta \approx \frac{Q^2}{\tilde{y}} \frac{\eta}{\xi} (1 + 2\tilde{K} \cos \varphi_\ell), \quad (35)$$

$$\begin{aligned} \ell_- \cdot k \approx & \frac{Q^2}{y\tilde{y}} \frac{1}{\xi} \left\{ \frac{1}{2}(\xi + \eta)(1 - \tilde{y}) + \frac{1}{2}(\xi - \eta)(1 - y) \right. \\ & \left. + \sigma \sqrt{(1 - y)(1 - \tilde{y})(\xi^2 - \eta^2)} \cos(\varphi_\gamma - \varphi_\ell) + 2\eta K \cos \varphi_\gamma + 2\eta \tilde{K} \cos \varphi_\ell \right\}. \end{aligned} \quad (36)$$

with

$$\left\{ \begin{array}{c} K \\ \tilde{K} \end{array} \right\} \approx -\frac{1}{2\eta} \sqrt{-\xi \frac{\Delta^2}{Q^2}} \sqrt{1 - \frac{\Delta_{\min}^2}{\Delta^2}} \sqrt{\frac{1 + \eta}{1 - \eta}} \times \left\{ \begin{array}{c} \sqrt{(1 - y)(\xi - \eta)} \\ \sqrt{(1 - \tilde{y})(\xi + \eta)} \end{array} \right\}. \quad (37)$$

We note that in Eq. (36) we replaced the original square root $\sqrt{(1-y)(1-\tilde{y})(1-\eta^2/\xi^2)Q^4}$ in front of $\cos(\varphi_\gamma - \varphi_\ell)$ by $\sigma Q^2/\xi \sqrt{(1-y)(1-\tilde{y})(\xi^2 - \eta^2)}$, since Q^2/ξ is positive for the kinematics we are considering, σ is $+1$. However, below in discussion of relations between the amplitudes we will make use of exchange symmetries that induce the interchange $\xi \rightarrow -\xi$ and $Q^2 \rightarrow Q^2$ in the underlying formulas. Under these substitutions, σ changes the sign and takes the negative value -1 . Making use of the results, we have just derived, we are now in a position to proceed with the computation of amplitudes. Before doing this, let us discuss in the next section factorization properties and the structure of the virtual Compton scattering amplitude.

3 Factorization of Compton amplitude

The amplitude \mathcal{T}_{VCS} is the object of interest since it involves the off-forward Compton scattering amplitude on the nucleon $T_{\mu\nu}$. This tensor

$$T_{\mu\nu} = i \int d^4z e^{iq \cdot z} \langle p_2 | T \{ j_\mu(z/2) j_\nu(-z/2) \} | p_1 \rangle \quad (38)$$

is expressed as a hadronic matrix element of the time-ordered product of the two quark electromagnetic currents

$$j_\mu(z) = \sum_q Q_q \bar{\psi}_q(z) \gamma_\mu \psi_q(z). \quad (39)$$

Here we extracted the absolute value of the electron charge so that Q_q is the quark's fractional charge.

3.1 Structure of amplitudes in the generalized Bjorken limit

Let us demonstrate the factorization of the VCS amplitude using the example of a cubic scalar model¹. Although theorems of this sort already exist in the literature [3, 13], it is rather instructive to have a fresh inspection. We only need to analyze the singularity structure stemming from the denominators of particle propagators. Numerators present in QCD case will not be relevant for our present needs. Complications due to the gauge invariance in the realistic case will be treated in a straightforward manner. We will disregard throughout the contribution of crossed diagrams since they do not bring any new insights into the factorization property of the hadronic tensor.

The tree-level Compton amplitude, see Fig. 3 (a), reads

$$T_{(0)} = \frac{1}{(p_1 + q_1)^2 + i0} = \frac{1}{(p \cdot q)} \frac{1}{1 - \xi + \frac{1}{2}\epsilon + i0}, \quad (40)$$

¹The absence of a stable vacuum state in this model is irrelevant for the demonstration of generic perturbative properties of scattering amplitudes.

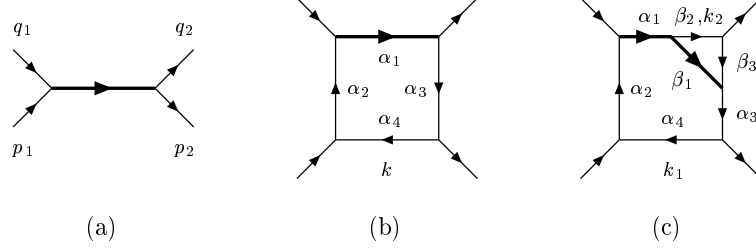


Figure 3: Lowest order perturbative diagrams exhibiting possible short-distance regimes contributing to the asymptotics of Compton scattering amplitude. Thick lines correspond to the highly virtual propagators.

where the small correction to the scaling contribution is $\epsilon \equiv (2M_N^2 - \Delta^2/2)/(p \cdot q)$. From here it is obvious that the expansion parameter is $1/(p \cdot q) = \xi/Q^2$, not Q^2 as it is suggested by the definition (38). Actually, this scale approaches zero when the virtualities of incoming and outgoing photons are of the same magnitude. When $p \cdot q \rightarrow \infty$ and ξ is fixed, one recovers the scaling coefficient function $1/(x - \xi + i0)$ convoluted with the “perturbative” GPD which, to this order, is $H_{(0)}(x, \eta, \Delta^2) = \delta(1 - x)$.

The one-loop expression for the amplitude displayed in Fig. 3 (b) is

$$T_{(1)} = ig^2 \int \frac{d^4 k}{(2\pi)^4} \frac{1}{k^2 (k + p_1)^2 (k + p_2)^2 (k + p_1 + q_1)^2} = \frac{g^2}{(4\pi)^2} \int_0^\infty \prod_{j=1}^4 d\alpha_j \frac{e^{i(E_1 + i0_\alpha)}}{\alpha^2}, \quad (41)$$

($0_\alpha \equiv 0 \cdot \alpha$) where

$$E_1 = \alpha_1 \left\{ \left(1 - \xi + \frac{1}{2}\epsilon\right) \left(1 - \frac{\alpha_1}{\alpha}\right) - (1 - \eta + \epsilon) \frac{\alpha_2}{\alpha} - (1 + \eta + \epsilon) \frac{\alpha_3}{\alpha} \right\} (p \cdot q) + \frac{\alpha_2 \alpha_3}{\alpha} \Delta^2 + (\alpha_2 + \alpha_3) \left(1 - \frac{\alpha_2 + \alpha_3}{\alpha}\right) M_N^2, \quad (42)$$

and $\alpha \equiv \sum_{j=1}^4 \alpha_j$. Integrating in the vicinity of $\alpha_1 \rightarrow 0$, which corresponds to the large virtuality of the corresponding line in the Feynman diagram, — the propagator between the photon vertices, — one gets, to leading order in $1/(p \cdot q)$, the contribution

$$T_{(1)}^{\text{SD1}} = \frac{1}{(p \cdot q)} \int_{-1}^1 dx \frac{H_{(1)}(x, \eta, \Delta^2)}{x - \xi + i0}, \quad (43)$$

where we introduced the one-loop GPD, which absorbs mass singularities,

$$H_{(1)}(x, \eta, \Delta^2) = \frac{ig^2}{(4\pi)^2} \int_0^\infty \prod_{j=2}^4 d\alpha_j \delta \left(x - 1 + (1 - \eta) \frac{\alpha_2}{\tilde{\alpha}} + (1 + \eta) \frac{\alpha_3}{\tilde{\alpha}} \right) \frac{e^{i(\tilde{E}_1 + i0_{\tilde{\alpha}})}}{\tilde{\alpha}^2} \quad (44)$$

Here $\tilde{\alpha} = \alpha_2 + \alpha_3 + \alpha_4$ and $\tilde{E}_1 = E_1[\alpha_1 = 0]$ does not depend on large scales. Summing the tree and one-loop contributions, one gets the factorized expression of the form (43) with $H_{(1)}$ being replaced

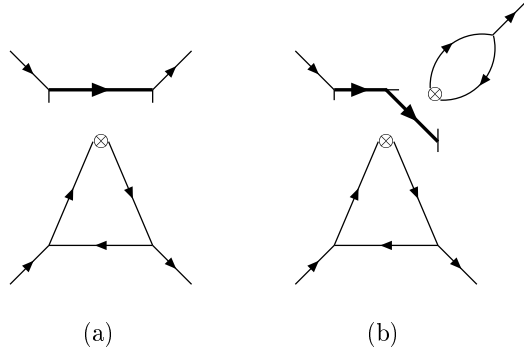


Figure 4: Short-distance regimes corresponding to loop diagrams in Fig. 3.

by $H = H_{(0)} + H_{(1)} + \dots$. One can easily convince oneself that the aforementioned perturbative expansion of the GPD $H(x, \eta, \Delta^2)$ arises from the light-cone operators matrix element:

$$H(x, \eta, \Delta^2) = p_+ \int \frac{d\xi_-}{2\pi} e^{ix\xi_- p_+} \langle p_2 | \phi(-\xi_-, 0_+, \mathbf{0}) \phi(\xi_-, 0_+, \mathbf{0}) | p_1 \rangle. \quad (45)$$

We refer to appendix A for the definition of the light-cone vectors.

Other short-distance and infrared regimes lead to power-suppressed contributions compared to the leading one (43), see Ref. [3]. More particle attachments from the hadronic line to the hard propagator obviously lead to a stronger dumping of amplitudes, except for the effect of longitudinally polarized gauge bosons in gauge field theories. The latter restore the gauge invariance of the naive GPD (45), with the ϕ -scalars begin replaced by the quark fields ψ . The analysis of the most general hand-bag diagram, i.e., with a single propagator between the photon vertices, does not bring new complications compared to the already discussed one-loop example and can be treated in an analogous manner. In QCD case, due to the fact that quarks are fermions, the numerators of their propagators cancel the power of $p \cdot q$ stemming from the denominator, so that $T^{\text{SD1}} \sim \mathcal{O}(p \cdot q^0)$.

Due to the timelike nature of the final-state photon virtuality, the quark-antiquark pair can form an on-shell intermediate hadronic state before annihilating into the heavy photon. This happens when the hard momentum is re-routed around the photon vertex as demonstrated in the diagram 3 (c). This configuration can potentially generate leading asymptotic behavior when the photon virtuality is low. Let us demonstrate that it is actually suppressed. The two-loop diagram 3 (c) has the form

$$T_{(3)} = -g^4 \int \frac{d^4 k_1}{(2\pi)^4} \frac{1}{k_1^2 (k_1 + p_1)^2 (k_1 + p_2)^2 (k_1 + p_1 + p_2)^2} \times \int \frac{d^4 k_2}{(2\pi)^4} \frac{1}{k_2^2 (k_2 - q_2)^2 (k_2 - k_1 - q_1 - p_1)^2} = i \frac{g^4}{(4\pi)^4} \int_0^\infty \prod_{i=1}^4 d\alpha_i \prod_{j=1}^3 d\beta_j \frac{e^{i(E_2 + i0_{\alpha+\beta})}}{[\alpha\beta + \beta_1(\beta - \beta_1)]^2} \quad (46)$$

with $\alpha \equiv \sum_{i=1}^4 \alpha_i$, $\beta \equiv \sum_{i=1}^3 \beta_i$. The exponential reads

$$\begin{aligned}
E_2 = & \alpha \frac{\alpha_1 + \beta_1 \left(1 - \frac{\beta_1 + \beta_3}{\beta}\right)}{\alpha + \beta_1 \left(1 - \frac{\beta_1}{\beta}\right)} \\
& \times \left\{ (1 - \xi + \tfrac{1}{2}\epsilon) \left(1 - \frac{\alpha_1}{\alpha} + \frac{\beta_1 \beta_3}{\alpha \beta}\right) - (1 - \eta + \epsilon) \frac{\alpha_2}{\alpha} - (1 + \eta + \epsilon) \left(\frac{\alpha_3}{\alpha} + \frac{\beta_1 \beta_3}{\alpha \beta}\right) \right\} (p \cdot q) \\
& + \frac{\alpha_2 \left(\alpha_3 + \frac{\beta_1 \beta_3}{\beta}\right)}{\alpha + \beta_1 \left(1 - \frac{\beta_1}{\beta}\right)} \Delta^2 + \left(\alpha_2 + \alpha_3 + \frac{\beta_1 \beta_3}{\beta}\right) \left(1 - \frac{\alpha_2 + \alpha_3 + \frac{\beta_1 \beta_3}{\beta}}{\alpha + \beta_1 \left(1 - \frac{\beta_1}{\beta}\right)}\right) M_N^2 \\
& + \beta_3 \left(1 - \frac{\beta_1 + \beta_3}{\beta}\right) M_{\ell\ell}^2.
\end{aligned} \tag{47}$$

In the short-distance regime, i.e., $\alpha_1 \rightarrow 0$, $\beta_1 \rightarrow 0$, where we define $\tilde{\alpha} = \alpha_2 + \alpha_3 + \alpha_4$ and $\tilde{\beta} = \beta_2 + \beta_3$, we get, see Fig. 4 (b),

$$T_{(3)}^{\text{SD2}} = -\frac{g^2}{(p \cdot q)^2} \int_{-1}^1 dx \int_0^1 du \frac{H_{(1)}(x, \eta, \Delta^2) \Pi_{(1)}(u, M_{\ell\ell}^2)}{(1-u)(x-\xi+i0)^2}, \tag{48}$$

where $H_{(1)}$ was given above, since $\tilde{E}_1 = E_2[\alpha_1 = \beta_i = 0]$, while

$$\Pi_{(1)}(u, M_{\ell\ell}^2) = \frac{1}{(4\pi)^2} \int_0^\infty \prod_{j=2}^3 d\beta_j \delta\left(u - \frac{\beta_3}{\beta}\right) \exp\left\{i\beta_3 \left(1 - \frac{\beta_3}{\beta}\right) M_{\ell\ell}^2\right\} \tag{49}$$

is the first term in the perturbative expansion of the correlation function

$$\Pi(u, M_{\ell\ell}^2) = iq_{2-} \int d^4 z e^{iq_2 \cdot z} \int \frac{d\xi_+}{2\pi} e^{-iu\xi_+ + q_{2-}} \langle 0 | T \{ \phi(0_-, 0_+, \mathbf{0}) \phi(0_-, \xi_+, \mathbf{0}), j(z) \} | 0 \rangle, \tag{50}$$

where the “electromagnetic” current is $j(z) = \frac{1}{2}\phi^2(z)$. Therefore, we observe that this short-distance regime is suppressed compared to the leading one, Eq. (43).

In the QCD case, the suppression of contributions due to the hadronic component of the photon is much milder than in the scalar example and it is only $(p \cdot q)^{-1/2}$ compared to the handbag diagram. The structure of the reduced amplitude is the same as in Eq. (48), however with only one power of the hard-scattering coefficient $1/(x-\xi+i0)$ being involved and the vacuum correlator is of the form

$$\begin{aligned}
\Pi_\mu(u, q_2) & \equiv (q_{2\mu} q_{2\nu} - M_{\ell\ell}^2 g_{\mu\nu}) n_\nu^* \Pi(u, M_{\ell\ell}^2) \\
& = i \int d^4 z e^{iz \cdot q_2} \int \frac{d\xi_+}{2\pi} e^{-iu\xi_+ + q_{2-}} \langle 0 | T \{ \bar{\psi}(0_-, 0_+, \mathbf{0}) \gamma_- \psi(0_-, \xi_+, \mathbf{0}), j_\mu(z) \} | 0 \rangle.
\end{aligned} \tag{51}$$

The correlation function can be saturated by the ρ -meson and reads

$$\Pi(u, M_{\ell\ell}^2) = -\frac{m_\rho^2}{g_\rho^2} \frac{\varphi_\rho(u)}{M_{\ell\ell}^2 - m_\rho^2 + im_\rho \Gamma_\rho} + \frac{3}{4\pi^2} u(1-u) \int_{s_0}^\infty \frac{ds}{s - M_{\ell\ell}^2 - i0}, \tag{52}$$

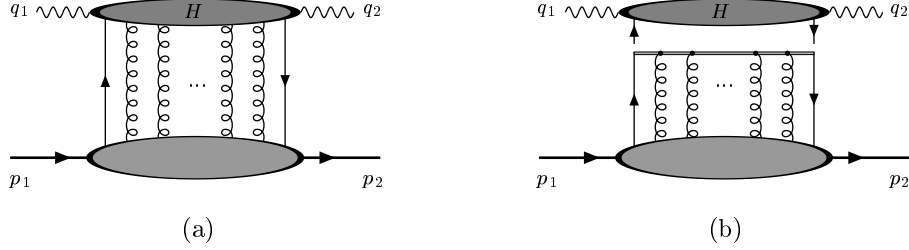


Figure 5: The leading asymptotic region in the Compton scattering amplitude (a) and the factorization of longitudinal gluons into the path-ordered exponential (b).

where $\varphi_\rho(u)$ is the ρ -meson distribution amplitude normalized according to $\int_0^1 du \varphi_\rho(u) = 1$, while $g_\rho^2/(4\pi) = 2.36 \pm 0.18$, $m_\rho = 770$ MeV and $\Gamma_\rho = 150$ MeV are the ρ -meson decay constant, mass and width, respectively. The second term on the right-hand side comes from the perturbative contribution to the correlator, known to two-loop order [14], a part of which is dual to the ρ -meson in the interval $s \in [0, s_0]$ and is absorbed there. The parameter $s_0 \approx 0.8 \text{ GeV}^2$ is the continuum threshold². Due to divergence in the correlation function, one has to use a renormalized expression, stemming from the subtracted dispersion relation, $\Pi_R(u, M_{\ell\bar{\ell}}^2) = \Pi(u, M_{\ell\bar{\ell}}^2) - \Pi(u, 0)$. The gauge invariance of the light-ray operator involved in the correlation function is restored by means of Wilson lines as discussed below.

From this result it is apparent that there is an extra imaginary part, besides the conventional s -channel discontinuity, in the VCS amplitude associated with the production of an on-shell intermediate hadronic state by the quark-antiquark pair. Due to the current conservation, which implies $\bar{u}(\ell_-)\not{q}_2 u(-\ell_+) = 0$, only one Lorentz structure contributes to the lepton production amplitude so that

$$\Pi_\mu(u, q_2) \frac{g_{\mu\nu}}{M_{\ell\bar{\ell}}^2} \bar{u}(\ell_-) \gamma_\nu u(-\ell_+) = -\Pi(u, M_{\ell\bar{\ell}}^2) \bar{u}(\ell_-) \gamma_- u(-\ell_+). \quad (53)$$

We should note, that due to the inequality, in general, of the skewness and the generalized Bjorken variable $\eta \neq \mp\xi$, possible complications due to the singular structure of the hard coefficient function do not arise since the pole in the former is away from the “turning” point in GPDs when one of the struck partons has zero momentum fraction. Moreover, it was demonstrated that GPDs are continuous at this point, i.e., have no jumps, so that the region does not present a problem in the case $\eta = \mp\xi$ either [3, 15, 13].

We finally conclude that the leading region in the amplitude is depicted in Fig. 5 (a), where in addition to considerations of the scalar theory, one is allowed to attach an infinite number of zero-twist longitudinally polarized gluons to the hard part. They do not induce power suppressed

²The approximation of the continuum contribution by a step-function threshold in the spectral density causes a divergence in the real part at $M_{\ell\bar{\ell}}^2 = s_0$, which is spurious.

contributions and factorize into the Wilson line along the trajectory of motion of the struck quark in the hard subprocess, see Refs. [16, 17, 18] and [19] for the most recent and complete treatment of this issue. As a result the quark field in the naive definition of the GPD gets replaced by

$$\psi(y_-, 0_+, \mathbf{0}) \rightarrow P \exp \left(ig \int_{y_-}^{\infty} dz_- A_+(z_-, 0_-, \mathbf{0}) \right) \psi(y_-, 0, \mathbf{0}). \quad (54)$$

Due to the unitary cancellation of the eikonal lines beyond the photon absorption and emission points, the path-ordered exponential extends only between the quark fields, see Fig. 5 (b).

3.2 Lorentz decomposition of Compton amplitude

The gauge invariant decomposition of the hadronic tensor (38) was found in Ref. [20] by an explicit twist-three analysis at leading order of perturbation theory [see Refs. [21, 22, 23] for independent developments along this line]. Presently, we concentrate on the twist-two sector at leading order in QCD coupling constant. As a consequence, we will not discuss gluonic contributions, in particular helicity-flip gluon effects which introduce new Lorentz structures into the hadronic tensor. The Compton scattering amplitude $T_{\mu\nu}$ admits the following Lorentz invariant decomposition in terms of Compton form factors (CFFs)

$$\begin{aligned} T_{\mu\nu} = & -\frac{1}{2} \left(g_{\mu\nu} - \frac{q_{1\mu} q_{2\nu}}{q_1 \cdot q_2} \right) \mathcal{V}_1(\xi, \eta, \Delta^2) + \frac{1}{2p \cdot q} \left(p_\mu - \frac{p \cdot q_2}{q_1 \cdot q_2} q_{1\mu} \right) \left(p_\nu - \frac{p \cdot q_1}{q_1 \cdot q_2} q_{2\nu} \right) \mathcal{V}_2(\xi, \eta, \Delta^2) \\ & + \frac{i}{2p \cdot q} \varepsilon_{\theta\lambda\rho\sigma} p_\rho q_\sigma \left(g_{\mu\theta} - \frac{p_\mu q_{2\theta}}{p \cdot q_2} \right) \left(g_{\nu\lambda} - \frac{p_\nu q_{1\lambda}}{p \cdot q_1} \right) \mathcal{A}(\xi, \eta, \Delta^2). \end{aligned} \quad (55)$$

Here $\varepsilon^{0123} = 1$. To simplify notations we will set in what follows $\mathcal{V}_1 \equiv \mathcal{V}$ and use the longitudinal-longitudinal helicity³ amplitude

$$\mathcal{V}_L \equiv \frac{1}{\xi} \mathcal{V}_2 - \mathcal{V}_1 \quad (56)$$

analogous to the longitudinal structure function F_L of deeply inelastic scattering.

The Compton form factors are decomposed into Dirac structures via

$$\mathcal{V} = h_+ \mathcal{H} + e_+ \mathcal{E}, \quad \mathcal{V}_L = h_+ \mathcal{H}_L + e_+ \mathcal{E}_L, \quad \mathcal{A} = \tilde{h}_+ \tilde{\mathcal{H}} + \tilde{e}_+ \tilde{\mathcal{E}}. \quad (57)$$

with Dirac bilinears which read

$$\begin{aligned} h_\mu &= \bar{u}(p_2) \gamma_\mu u(p_1), & e_\mu &= \bar{u}(p_2) i \sigma_{\mu\nu} \frac{\Delta_\nu}{2M_N} u(p_1), \\ \tilde{h}_\mu &= \bar{u}(p_2) \gamma_\mu \gamma_5 u(p_1), & \tilde{e}_\mu &= \frac{\Delta_\mu}{2M_N} \bar{u}(p_2) \gamma_5 u(p_1), \end{aligned} \quad (58)$$

³Referring to incoming-outgoing virtual photons.

where u is the nucleon bispinor normalized as $\bar{u}(p)u(p) = 2M_N$ and $\gamma_5 = \begin{pmatrix} 0 & 1 \\ 1 & 0 \end{pmatrix}$.

As we demonstrated in the previous section, the inverse s -channel energy $p \cdot q$ sets the distance between the quark fields in the Compton scattering amplitude. Therefore, for the QCD factorization to be applicable one has to impose the condition

$$(p \cdot q) \gg \max\{M_N^2, |\Delta^2|\}. \quad (59)$$

In this domain, the Compton form factors are factorized, as we have shown above, into calculable coefficient functions and GPDs via, cf. (43),

$$\begin{aligned} (\mathcal{H}, \mathcal{E})(\xi, \eta, \Delta^2) &= \sum_{i=u,d,s,G} \int_{-1}^1 dx C_i^{(-)}(x, \xi) (H_i, E_i)(x, \eta, \Delta^2), \\ (\widetilde{\mathcal{H}}, \widetilde{\mathcal{E}})(\xi, \eta, \Delta^2) &= \sum_{i=u,d,s,G} \int_{-1}^1 dx C_i^{(+)}(x, \xi) (\widetilde{H}_i, \widetilde{E}_i)(x, \eta, \Delta^2), \end{aligned} \quad (60)$$

where the sum runs over all parton species. Analogous factorized formula holds for \mathcal{H}_L and \mathcal{E}_L with the coefficient function $C^{(-)}(x, \xi)$ being replaced by $C_L(x, \xi)$. To zeroth-order in the QCD coupling constant only the quark coefficient functions $i = q$

$$C_q^{(\mp)}(x, \xi) = \frac{Q_q^2}{\xi - x - i0} \mp \frac{Q_q^2}{\xi + x - i0} + \mathcal{O}(\alpha_s), \quad (61)$$

give a nonvanishing contribution. The Compton form factor \mathcal{V}_L does not enter in leading order. This is a consequence of a (generalized) Callan-Gross relation, $\mathcal{V}_2 = \xi \mathcal{V}_1 + \mathcal{O}(\alpha_s)$. Thus, $C_L(x, \xi)$ starts at next-to-leading order, i.e., $\mathcal{O}(\alpha_s)$, as we emphasized above. Perturbative corrections to $C_q^{(\pm)}$ and gluon contributions are available at one-loop order [24, 25, 26, 27, 28].

4 Cross section

This section is devoted to the calculation of the electroproduction cross section with the leading-twist Compton scattering amplitude analyzed above. In the next section we compute a generic form of the squared amplitude, where the hadronic part is left untouched and the leptonic sector is fully worked out. Then this intermediate result is used in section 4.2 for the evaluation of the cross section for an unpolarized nucleon and is further used for deriving the results in appendix B, when the polarization of the target is available as an option.

4.1 Generating function

The square of the total amplitude, $\mathcal{T} = \mathcal{T}_{\text{VCS}} + \mathcal{T}_{\text{BH}_1} + \mathcal{T}_{\text{BH}_2}$, involves three essentially different contributions

$$\mathcal{T}^2 = |\mathcal{T}_{\text{VCS}}|^2 + \mathcal{I} + |\mathcal{T}_{\text{BH}_1} + \mathcal{T}_{\text{BH}_2}|^2, \quad (62)$$

the square of the virtual Compton scattering amplitude, — bilinear in Compton form factors, — the square of the Bethe-Heitler processes, — independent on GPDs and expressed solely in terms of elastic form factors, — and, at last, the interference term

$$\mathcal{I} = \mathcal{T}_{\text{VCS}}\mathcal{T}_{\text{BH}_1}^\dagger + \mathcal{T}_{\text{VCS}}\mathcal{T}_{\text{BH}_2}^\dagger + \mathcal{T}_{\text{VCS}}^\dagger\mathcal{T}_{\text{BH}_1} + \mathcal{T}_{\text{VCS}}^\dagger\mathcal{T}_{\text{BH}_2}, \quad (63)$$

which is linear in Compton form factors.

For the electron beam, the separate contributions to the total amplitude read

$$\mathcal{T}_{\text{VCS}} = \frac{e^4}{q_1^2 q_2^2} \bar{u}(\ell_-)\gamma_\mu u(-\ell_+) \bar{u}(k')\gamma_\nu u(k) T_{\mu\nu}, \quad (64)$$

$$\mathcal{T}_{\text{BH}_1} = \frac{e^4}{q_2^2 \Delta^2} \bar{u}(\ell_-)\gamma_\mu u(-\ell_+) \bar{u}(k') \left(\gamma_\mu \frac{1}{\not{k} - \not{\Delta}} \gamma_\nu + \gamma_\nu \frac{1}{\not{k}' + \not{\Delta}} \gamma_\mu \right) u(k) J_\nu, \quad (65)$$

$$\mathcal{T}_{\text{BH}_2} = \frac{e^4}{q_1^2 \Delta^2} \bar{u}(k')\gamma_\mu u(k) \bar{u}(\ell_-) \left(\gamma_\mu \frac{1}{-\not{\ell}_+ - \not{\Delta}} \gamma_\nu + \gamma_\nu \frac{1}{\not{\ell}_- + \not{\Delta}} \gamma_\mu \right) u(-\ell_+) J_\nu, \quad (66)$$

corresponding to diagrams (a), (b), and (c) in Fig. 1, respectively, including the crossed contributions in the latter two cases. The VCS tensor $T_{\mu\nu}$ was given previously in Eq. (55), while the nucleon electromagnetic current is parametrized in terms of the Dirac and Pauli form factors

$$J_\mu \equiv \langle p_2 | j_\mu(0) | p_1 \rangle = F_1(\Delta^2) h_\mu + F_2(\Delta^2) e_\mu, \quad (67)$$

using the bilinears from (58). The two amplitudes \mathcal{T}_{VCS} and $\mathcal{T}_{\text{BH}_2}$ change the overall sign when one switches from the electron to the positron beam, and so do the interference terms involving them, while the $\mathcal{T}_{\text{BH}_1}$ does not. Obviously, both BH amplitudes are related by the interchange of the momenta $k' \leftrightarrow \ell_-$ and $k \leftrightarrow -\ell_+$. Moreover, we find that the VCS and the first BH amplitude are even under the interchange of the produced leptons in the pair, while the second BH amplitude is odd. This symmetry property in the timelike DVCS plays an analogous role as the charge asymmetry in the spacelike case [10].

The evaluation of separate terms yields expressions which are represented as a Fourier sum of a few harmonics in the difference of the azimuthal angles $\varphi_l - \varphi_\gamma = \varphi_l - \phi - \pi$. Namely, we get for particular contributions to the total amplitude squared.

- The VCS amplitude squared

$$|\mathcal{T}_{\text{VCS}}|^2 = \frac{2\xi^2 e^8}{Q^4 y^2 \tilde{y}^2 (\eta^2 - \xi^2)} \sum_{n=0}^2 \left(a_n^{\text{VCS}} + \lambda b_n^{\text{VCS}} \right) \cos(n(\varphi_l - \phi)), \quad (68)$$

has the following expansion coefficients

$$a_0^{\text{VCS}} = \frac{1}{2} (2 - 2y + y^2) (2 - 2\tilde{y} + \tilde{y}^2) \left(\mathcal{V}\mathcal{V}^\dagger + \mathcal{A}\mathcal{A}^\dagger \right) + 4(1 - y)(1 - \tilde{y}) \frac{\xi^2 - \eta^2}{\xi^2} \mathcal{V}_L \mathcal{V}_L^\dagger, \quad (69)$$

$$a_1^{\text{VCS}} = -\frac{\sigma}{\xi} \sqrt{(1 - y)(1 - \tilde{y})(\xi^2 - \eta^2)} (2 - y)(2 - \tilde{y}) \left(\mathcal{V}\mathcal{V}_L^\dagger + \mathcal{V}_L \mathcal{V}^\dagger \right), \quad (70)$$

$$a_2^{\text{VCS}} = 2(1-y)(1-\tilde{y}) \left(\mathcal{V}\mathcal{V}^\dagger - \mathcal{A}\mathcal{A}^\dagger \right), \quad (71)$$

$$b_0^{\text{VCS}} = \frac{1}{2}y(2-y)(2-2\tilde{y}+\tilde{y}^2) \left(\mathcal{V}\mathcal{A}^\dagger + \mathcal{A}\mathcal{V}^\dagger \right), \quad (72)$$

$$b_1^{\text{VCS}} = -\frac{\sigma}{\xi} \sqrt{(1-y)(1-\tilde{y})(\xi^2 - \eta^2)y(2-\tilde{y})} \left(\mathcal{V}_L\mathcal{A}^\dagger + \mathcal{A}\mathcal{V}_L^\dagger \right), \quad (73)$$

$$b_2^{\text{VCS}} = 0. \quad (74)$$

Note that contrary to the DVCS case, due to the virtuality of both the incoming and outgoing photons, the Lorentz structure accompanying \mathcal{V}_L does indeed contribute to the cross section and generates, e.g., the coefficient a_1^{VCS} .

The interference of the VCS amplitude with the BH ones will involve lepton propagators from the latter which will bring [conveniently rescaled] factors in the denominator

$$(k' + \Delta)^2 \equiv -2\eta p \cdot q \mathcal{P}_1(k), \quad (k - \Delta)^2 \equiv -2\eta p \cdot q \mathcal{P}_2(k), \quad (75)$$

$$(\ell_+ + \Delta)^2 \equiv 2\eta p \cdot q \mathcal{P}_3(\ell_-), \quad (\ell_- + \Delta)^2 \equiv 2\eta p \cdot q \mathcal{P}_4(\ell_-). \quad (76)$$

The expressions are rather lengthy and are obtained by means of substitution of Eqs. (24) and (26) into the left-hand side of the above definitions. We also introduce the following shorthand notations for the structures involving the nucleon matrix element of the quark electromagnetic current to make the formulas look as concise as possible,

$$\mathcal{S}_1 \equiv \eta \left(k - \frac{1}{y}q_1 \right) \cdot J^\dagger - \frac{1}{p \cdot q} \left(k - \frac{1}{y}q_1 \right) \cdot \Delta \, q_1 \cdot J^\dagger, \quad (77)$$

$$\mathcal{S}_2 \equiv \eta \left(\ell_- - \frac{1}{\tilde{y}}q_2 \right) \cdot J^\dagger - \frac{1}{p \cdot q} \left(\ell_- - \frac{1}{\tilde{y}}q_2 \right) \cdot \Delta \, q_2 \cdot J^\dagger, \quad (78)$$

$$\mathcal{R}_1 \equiv \frac{i}{p \cdot q} \epsilon_{\mu\nu\rho\sigma} q_\mu k_\nu \Delta_\rho J_\sigma^\dagger, \quad \mathcal{R}_2 \equiv \frac{i}{p \cdot q} \epsilon_{\mu\nu\rho\sigma} q_\mu \ell_{-\nu} \Delta_\rho J_\sigma^\dagger. \quad (79)$$

With these results at hand, we find, similarly to the previous analysis of $|\mathcal{T}_{\text{VCS}}|^2$, the interference contributions from the VCS and BH amplitudes.

- The interference $\mathcal{T}_{\text{VCS}}\mathcal{T}_{\text{BH}_1}^\dagger$:

$$\mathcal{T}_{\text{VCS}}\mathcal{T}_{\text{BH}_1}^\dagger = \frac{2\xi^2 e^8}{y^2 \tilde{y}^2 \eta^2 (\eta^2 - \xi^2) Q^4 \Delta^2 \mathcal{P}_1(k) \mathcal{P}_2(k)} \sum_{n=0}^2 \left(a_n^1 + \lambda b_n^1 \right) \cos \left(n(\varphi_l - \phi) \right), \quad (80)$$

where

$$\begin{aligned} a_0^1 = & 4(1-y)(1-\tilde{y}) \left(\eta \mathcal{S}_1 \mathcal{V} - \xi \mathcal{R}_1 \mathcal{A} + 2 \frac{\xi^2 - \eta^2}{\xi} \mathcal{S}_1 \mathcal{V}_L \right) \\ & - (2-2y+y^2)(2-2\tilde{y}+\tilde{y}^2) \left(\xi \mathcal{S}_1 \mathcal{V} + \eta \mathcal{R}_1 \mathcal{A} \right) \\ & - 2 \frac{\tilde{y}}{y} (1-y)(2-y)(2-\tilde{y})(\xi - \eta) \left(\mathcal{R}_2 \mathcal{A} + \frac{\eta}{\xi} \mathcal{S}_2 \mathcal{V}_L \right), \end{aligned} \quad (81)$$

$$a_1^1 = 2\sigma\sqrt{(1-y)(1-\tilde{y})(\xi^2-\eta^2)} \quad (82)$$

$$\times \left\{ (2-y)(2-\tilde{y}) \left(\mathcal{S}_1\mathcal{V} + \mathcal{R}_1\mathcal{A} - \frac{\xi-\eta}{\xi}\mathcal{S}_1\mathcal{V}_L \right) - 4\frac{\tilde{y}}{y}\frac{1-y}{\xi+\eta}(\eta\mathcal{S}_2\mathcal{V} - \xi\mathcal{R}_2\mathcal{A}) \right\},$$

$$a_2^1 = -4(\xi-\eta)(1-y)(1-\tilde{y})(\mathcal{S}_1\mathcal{V} + \mathcal{R}_1\mathcal{A}), \quad (83)$$

$$b_0^1 = -y(2-y)(2-2\tilde{y}+\tilde{y}^2)(\xi\mathcal{S}_1\mathcal{A} + \eta\mathcal{R}_1\mathcal{V}) - 2(\xi-\eta)(1-y)\tilde{y}(2-\tilde{y})\mathcal{R}_2(\mathcal{V} + \mathcal{V}_L), \quad (84)$$

$$b_1^1 = 2\sigma\sqrt{(1-y)(1-\tilde{y})(\xi^2-\eta^2)}y(2-\tilde{y}) \left(\mathcal{S}_1\mathcal{A} + \mathcal{R}_1\mathcal{V} + \frac{\xi-\eta}{\xi}\mathcal{R}_1\mathcal{V}_L \right), \quad (85)$$

$$b_2^1 = 0. \quad (86)$$

• The interference $\mathcal{T}_{\text{VCS}}\mathcal{T}_{\text{BH}_2}^\dagger$:

$$\mathcal{T}_{\text{VCS}}\mathcal{T}_{\text{BH}_2}^\dagger = \frac{2\xi^2 e^8}{y^2\tilde{y}^2\eta^2(\eta^2-\xi^2)Q^4\Delta^2\mathcal{P}_3(\ell_-)\mathcal{P}_4(\ell_-)} \sum_{n=0}^2 (a_n^2 + \lambda b_n^2) \cos(n(\varphi_l - \phi)), \quad (87)$$

with

$$a_0^2 = 4(1-y)(1-\tilde{y}) \left(\eta\mathcal{S}_2\mathcal{V} - \xi\mathcal{R}_2\mathcal{A} - 2\frac{\xi^2-\eta^2}{\xi}\mathcal{S}_2\mathcal{V}_L \right) \\ + (2-2y+y^2)(2-2\tilde{y}+\tilde{y}^2)(\xi\mathcal{S}_2\mathcal{V} + \eta\mathcal{R}_2\mathcal{A}) \quad (88)$$

$$- 2\frac{y}{\tilde{y}}(1-\tilde{y})(2-y)(2-\tilde{y})(\xi+\eta) \left(\mathcal{R}_1\mathcal{A} + \frac{\eta}{\xi}\mathcal{S}_1\mathcal{V}_L \right),$$

$$a_1^2 = -2\sigma\sqrt{(1-y)(1-\tilde{y})(\xi^2-\eta^2)} \quad (89)$$

$$\times \left\{ (2-y)(2-\tilde{y}) \left(\mathcal{S}_2\mathcal{V} - \mathcal{R}_2\mathcal{A} - \frac{\xi+\eta}{\xi}\mathcal{S}_2\mathcal{V}_L \right) + 4\frac{y}{\tilde{y}}\frac{1-\tilde{y}}{\xi-\eta}(\eta\mathcal{S}_1\mathcal{V} - \xi\mathcal{R}_1\mathcal{A}) \right\},$$

$$a_2^2 = 4(\xi+\eta)(1-y)(1-\tilde{y})(\mathcal{S}_2\mathcal{V} - \mathcal{R}_2\mathcal{A}), \quad (90)$$

$$b_0^2 = y(2-y)(2-2\tilde{y}+\tilde{y}^2)(\xi\mathcal{S}_2\mathcal{A} + \eta\mathcal{R}_2\mathcal{V}) - 2(\xi+\eta)\frac{y^2}{\tilde{y}}(2-\tilde{y})(1-\tilde{y})\mathcal{R}_1(\mathcal{V} + \mathcal{V}_L), \quad (91)$$

$$b_1^2 = -2\sigma\sqrt{(1-y)(1-\tilde{y})(\xi^2-\eta^2)}y(2-\tilde{y}) \left(\mathcal{S}_2\mathcal{A} - \mathcal{R}_2\mathcal{V} - \frac{\xi+\eta}{\xi}\mathcal{R}_2\mathcal{V}_L \right), \quad (92)$$

$$b_2^2 = 0. \quad (93)$$

The unpolarized parts of the two interference terms must obey a symmetry relation, since the BH amplitudes (65) and (66) are related by the exchange $k \leftrightarrow -\ell_+$ and $k' \leftrightarrow \ell_-$. Obviously, $q_1 \leftrightarrow -q_2$ under it, while the Bose symmetry ensures the invariance of the Compton amplitude (64) with respect to this replacement. As we mentioned above, all the amplitudes have definite symmetry properties under the permutation of leptons in the pair $\ell_- \leftrightarrow \ell_+$ and, thus, we take the advantages of combining both transformations together, the above with $k \leftrightarrow -\ell_-$ and $k' \leftrightarrow \ell_+$. From the definitions of the four-vectors (20) and (23) one can read off, after some algebra, the complete set of substitution rules

$$Q^2 \rightarrow Q^2, \quad \xi \rightarrow -\xi, \quad \sigma \rightarrow -\sigma, \quad \Delta \rightarrow \Delta, \quad \eta \rightarrow \eta, \quad y \leftrightarrow \tilde{y}, \quad \varphi_\ell \leftrightarrow \phi. \quad (94)$$

Next, we remark that the product of the BH propagators (75) and (76) obeys the symmetry relation

$$\mathcal{P}_3\mathcal{P}_4(Q^2, \Delta^2, \xi, \eta, y, \tilde{y}, \varphi_\ell) = \mathcal{P}_1\mathcal{P}_2(Q^2, \Delta^2, -\xi, \eta, \tilde{y}, y, \phi = \varphi_\ell). \quad (95)$$

The prefactors in the interference terms (80) and (87) are even under the transformation (94). Moreover, from the definitions (77), (78), and (79) we conclude also that $\mathcal{S}_1 \leftrightarrow -\mathcal{S}_2$; $\mathcal{R}_1 \leftrightarrow -\mathcal{R}_2$ with (94). Taking all of our results together, we deduce that the Fourier coefficients satisfy the equalities

$$a_n^2 = -a_n^1 \Big|_{\substack{\mathcal{S}_1 \leftrightarrow -\mathcal{S}_2; \mathcal{R}_1 \leftrightarrow -\mathcal{R}_2 \\ y \leftrightarrow \tilde{y}; \xi \leftrightarrow -\xi}}, \quad (96)$$

where \mathcal{V} and \mathcal{A} are even and odd functions in ξ , respectively. This property is a consequence of the definitions (57) and (60), where in the hard-scattering amplitude (61) one has to replace $\xi - i0$ by $-\xi + i0$.

4.2 Angular dependence of the cross section

After giving the generic expression for the total amplitude squared, we will elaborate the hadronic part and present the result as a Fourier expansion in terms of the azimuthal angles, ϕ of the recoiled nucleon and φ_ℓ of a lepton in the lepton pair. Before doing so, we write down the general angular decomposition of the squared amplitudes, which results from the Lorentz structure of the leptonic tensors contracted with the hadronic ones. The harmonics, appearing here, can be classified with respect to the underlying twist expansion of the hadronic tensor (38) and the Fourier coefficients are in one-to-one correspondence with helicity amplitudes, defined in the target rest frame. Extracting certain kinematical factors in order to match the normalization adopted for the leptonproduction cross section of a real photon in Ref. [9], the square of the VCS amplitude and its interference with the BH amplitudes as well as the squared BH amplitudes admit the following expansion in these azimuthal angles

$$|\mathcal{T}_{\text{VCS}}|^2 = \frac{2\xi^2 e^8}{Q^4 y^2 \tilde{y}^2 (\eta^2 - \xi^2)} \sum_{n=0}^2 \left\{ c_n^{\text{VCS}}(\varphi_\ell) \cos(n\phi) + s_n^{\text{VCS}}(\varphi_\ell) \sin(n\phi) \right\}, \quad (97)$$

$$\begin{aligned} \mathcal{I} = \frac{2\xi(1-\eta)e^8}{y^3 \tilde{y}^3 (\eta^2 - \xi^2) Q^2 \Delta^2} \sum_{n=0}^3 \left\{ \pm \frac{\tilde{y}}{\mathcal{P}_1 \mathcal{P}_2(\phi)} \left(c_n^1(\varphi_\ell) \cos(n\phi) + s_n^1(\varphi_\ell) \sin(n\phi) \right) \right. \\ \left. + \frac{y}{\mathcal{P}_3 \mathcal{P}_4(\varphi_\ell)} \left(c_n^2(\phi) \cos(n\varphi_\ell) + s_n^2(\phi) \sin(n\varphi_\ell) \right) \right\}, \end{aligned} \quad (98)$$

$$\begin{aligned} |\mathcal{T}_{\text{BH}}|^2 = -\frac{\xi(1-\eta)^2}{y^4 \tilde{y}^4 \Delta^2 Q^2 \eta (\eta^2 - \xi^2)} \left\{ \sum_{n=0}^4 \left\{ \frac{\tilde{y}^2}{\mathcal{P}_1^2 \mathcal{P}_2^2(\phi)} \left(c_n^{11}(\varphi_\ell) \cos(n\phi) + s_n^{11}(\varphi_\ell) \sin(n\phi) \right) \right. \right. \\ \left. \left. + \frac{y^2}{\mathcal{P}_3^2 \mathcal{P}_4^2(\varphi_\ell)} \left(c_n^{22}(\phi) \cos(n\varphi_\ell) + s_n^{22}(\phi) \sin(n\varphi_\ell) \right) \right\} \right\} \end{aligned} \quad (99)$$

$$\pm \sum_{n=0}^3 \frac{y\tilde{y}}{\mathcal{P}_1\mathcal{P}_2\mathcal{P}_3\mathcal{P}_4} \left(c_n^{12}(\varphi_\ell) \cos(n\phi) + s_n^{12}(\varphi_\ell) \sin(n\phi) \right) \Big\} \Big\} .$$

Here the $+$ ($-$) sign stands for the electron (positron) beam and in the expansion we have used the relation between the azimuthal angles $\varphi_\gamma = \pi + \phi$. In turn, the Fourier coefficients for the squared VCS term ($i = \text{VCS}$), the interference term with the first BH amplitude (65) ($i = 1$), and the squared BH amplitude (65) ($i = 11$) are expanded up to the second order harmonics in the azimuthal angle φ_ℓ of the lepton pair

$$\begin{aligned} c_n^i(\varphi_\ell) &= \sum_{m=0}^2 \left\{ cc_{nm}^i \cos(m\varphi_\ell) + cs_{nm}^i \sin(m\varphi_\ell) \right\} , \\ s_n^i(\varphi_\ell) &= \sum_{m=0}^2 \left\{ sc_{nm}^i \cos(m\varphi_\ell) + ss_{nm}^i \sin(m\varphi_\ell) \right\} . \end{aligned} \quad (100)$$

While for the interference of the second BH amplitude (66) with the VCS one ($i = 2$) and its square ($i = 22$), an analogous expansion is performed in terms of the azimuthal angle ϕ . The interference of both BH amplitudes ($i = 12$) is analogous to Eq. (100), however, it contains now a third order harmonics in the azimuthal angle φ_ℓ . The Fourier coefficients linearly depend on the polarization vector of the nucleon, see Eq. (B.3). At the edge of the phase space the overall coefficient in the BH amplitude gets corrected according to

$$\frac{(1-\eta)^2}{\eta^2 - \xi^2} \rightarrow \frac{\left(1 - \eta + \frac{\xi\Delta^2}{2Q^2}\right)^2}{\eta^2 - \left(1 - \frac{\Delta^2}{4Q^2}\right)^2 \xi^2} . \quad (101)$$

We emphasize that $1/(\eta^2 - \xi^2)$ expressions in the squared VCS (97) and interference (98) terms are corrected in analogous manner to ensure their correct behavior in the limits $Q^2 \rightarrow 0$ and $M_{\ell\ell}^2 \rightarrow 0$.

Finally, we remark that all BH propagators, defined in Eqs. (75) and (76), are even functions in the azimuthal angle φ :

$$\mathcal{P}_i(\varphi) = \mathcal{P}_i(2\pi - \varphi) \quad \text{for } i = \{1, \dots, 4\} , \quad (102)$$

and, thus, even and odd harmonics can be clearly separated from each other. It is also worth to mention that $\mathcal{P}_3\mathcal{P}_4$ as a function of the lepton-pair solid angles φ_ℓ and θ_ℓ satisfy the symmetry relation

$$\mathcal{P}_3\mathcal{P}_4(\theta_\ell, \varphi_\ell) = \mathcal{P}_3\mathcal{P}_4(\pi - \theta_\ell, \varphi_\ell + \pi) . \quad (103)$$

For later use, we mention that as a consequence of this symmetry the integration over $d\theta_\ell$ in a symmetric interval around the point $\theta_\ell = \pi/2$ gives for any definite symmetric moment in θ_ℓ the

following characteristic cos-Fourier expansions (for any number r)

$$\int_{\pi/2-\vartheta}^{\pi/2+\vartheta} d\cos\theta_\ell \frac{\tau(\theta_\ell)}{[\mathcal{P}_3\mathcal{P}_4]^r} = \sum_{n=0,1,2,\dots} \tau_n(\vartheta) \begin{Bmatrix} \cos([2n+1]\varphi_\ell) \\ \cos(2n\varphi_\ell) \end{Bmatrix} \quad \text{for} \quad \begin{Bmatrix} \tau(\theta_\ell) = -\tau(\pi - \theta_\ell) \\ \tau(\theta_\ell) = \tau(\pi - \theta_\ell) \end{Bmatrix}, \quad (104)$$

where $\vartheta \leq \frac{\pi}{2}$.

4.2.1 Squared virtual Compton amplitude

At leading twist, it turns out that $|\mathcal{T}_{\text{VCS}}|^2$ depends only on the harmonics $\cos(n(\varphi_\ell - \phi))$ with $n = 0, 1, 2$. Consequently, we find in this approximation, with the help of the addition theorem $\cos(n(\varphi_\ell - \phi)) = \cos(n\varphi_\ell)\cos(n\phi) + \sin(n\varphi_\ell)\sin(n\phi)$, the following relations between the Fourier coefficients:

$$\begin{aligned} \text{ss}_{nn}^{\text{VCS}} &\simeq \text{cc}_{nn}^{\text{VCS}}, \\ \text{sc}_{nm}^{\text{VCS}} &\simeq \text{cs}_{nm}^{\text{VCS}} \simeq 0, \\ \text{ss}_{nm}^{\text{VCS}} &\simeq \text{cc}_{nm}^{\text{VCS}} \simeq 0, \quad n \neq m. \end{aligned} \quad (105)$$

The nonvanishing Fourier coefficients $\text{cc}_{nn}^{\text{VCS}}$ can be easily evaluated from the generic Eqs. (69)-(74) and products of Compton form factors. For the unpolarized target one defines

$$\frac{1}{4}\mathcal{V}\mathcal{V}^\dagger \equiv \mathcal{C}_{\mathcal{V}\mathcal{V},\text{unp}}^{\text{VCS}}, \quad \frac{1}{4}\mathcal{V}\mathcal{A}^\dagger \equiv \mathcal{C}_{\mathcal{V}\mathcal{A},\text{unp}}^{\text{VCS}}, \quad \frac{1}{4}\mathcal{A}\mathcal{A}^\dagger \equiv \mathcal{C}_{\mathcal{A}\mathcal{A},\text{unp}}^{\text{VCS}}, \quad (106)$$

where the functions $\mathcal{C}(\mathcal{F}, \mathcal{F}^*)$ depend on the set of Compton form factors. For this case we find at leading order in $1/(p \cdot q)$

$$\mathcal{C}_{\mathcal{V}\mathcal{V},\text{unp}}^{\text{VCS}}(\mathcal{F}, \mathcal{F}^*) = (1 - \eta^2)\mathcal{H}\mathcal{H}^* - \eta^2(\mathcal{H}\mathcal{E}^* + \mathcal{E}\mathcal{H}^*) - \left(\frac{\Delta^2}{4M^2} + \eta^2\right)\mathcal{E}\mathcal{E}^*, \quad (107)$$

$$\mathcal{C}_{\mathcal{A}\mathcal{A},\text{unp}}^{\text{VCS}}(\mathcal{F}, \mathcal{F}^*) = (1 - \eta^2)\widetilde{\mathcal{H}}\widetilde{\mathcal{H}}^* - \eta^2(\widetilde{\mathcal{H}}\widetilde{\mathcal{E}}^* + \widetilde{\mathcal{E}}\widetilde{\mathcal{H}}^*) - \eta^2\frac{\Delta^2}{4M^2}\widetilde{\mathcal{E}}\widetilde{\mathcal{E}}^*, \quad (108)$$

$$\mathcal{C}_{\mathcal{V}\mathcal{A},\text{unp}}^{\text{VCS}}(\mathcal{F}, \mathcal{F}^*) = 0. \quad (109)$$

The spin-dependent results, including both longitudinally and transversely polarized target options, are presented in the appendix B.1.

Note that in the (spacelike) DVCS limit, i.e., when one sets $\eta \simeq -\xi$, we retrieve our previous result from Ref. [9]

$$\mathcal{C}_{\text{unp}}^{\text{DVCS}} \stackrel{\text{DVCS}}{=} \mathcal{C}_{\mathcal{V}\mathcal{V},\text{unp}}^{\text{VCS}} + \mathcal{C}_{\mathcal{A}\mathcal{A},\text{unp}}^{\text{VCS}},$$

and analogous relations for the polarized case, see Eq. (B.10). In this way, we find for the unpolarized target the following nonvanishing Fourier coefficients in the twist-two sector

$$\text{cc}_{00,\text{unp}}^{\text{VCS}} = 2(2 - 2y + y^2)(2 - 2\tilde{y} + \tilde{y}^2) \left\{ \mathcal{C}_{\mathcal{V}\mathcal{V},\text{unp}}^{\text{VCS}}(\mathcal{F}, \mathcal{F}^*) + \mathcal{C}_{\mathcal{A}\mathcal{A},\text{unp}}^{\text{VCS}}(\mathcal{F}, \mathcal{F}^*) \right\}$$

$$+\frac{16}{\xi^2}(1-y)(1-\tilde{y})(\xi^2-\eta^2)\mathcal{C}_{\mathcal{V}\mathcal{V},\text{unp}}^{\text{VCS}}(\mathcal{F}_L, \mathcal{F}_L^*), \quad (110)$$

$$\text{cc}_{11,\text{unp}}^{\text{VCS}} = \frac{4\sigma}{\xi} \sqrt{(1-y)(1-\tilde{y})(\xi^2-\eta^2)(2-y)(2-\tilde{y})} \left\{ \mathcal{C}_{\mathcal{V}\mathcal{V},\text{unp}}^{\text{VCS}}(\mathcal{F}, \mathcal{F}_L^*) + \mathcal{C}_{\mathcal{V}\mathcal{V},\text{unp}}^{\text{VCS}}(\mathcal{F}_L, \mathcal{F}^*) \right\} \quad (111)$$

$$\text{cc}_{22,\text{unp}}^{\text{VCS}} = 8(1-y)(1-\tilde{y}) \left\{ \mathcal{C}_{\mathcal{V}\mathcal{V},\text{unp}}^{\text{VCS}}(\mathcal{F}, \mathcal{F}^*) - \mathcal{C}_{\mathcal{A}\mathcal{A},\text{unp}}^{\text{VCS}}(\mathcal{F}, \mathcal{F}^*) \right\}. \quad (112)$$

All other coefficients are expressed making use of Eq. (105). Note, however, that the tensor-gluon contribution induces further second order harmonics, which are not displayed here since they are suppressed by a power of α_s . The Fourier coefficients for the polarized target are collected in the appendix B.1.

4.2.2 Interference of virtual Compton and Bethe-Heitler amplitudes

In the leading-twist approximation the following general relations between the Fourier coefficients of the interference term are established

$$\begin{aligned} \text{ss}_{nm}^{\text{INT}} &\simeq \text{cc}_{nm}^{\text{INT}} \quad \text{and} \quad \text{cs}_{nm}^{\text{INT}} \simeq -\text{sc}_{nm}^{\text{INT}} \quad \text{for} \quad \{nm\} = \{12, 21, 32\}, \\ \text{ss}_{nm}^{\text{INT}} &\simeq \text{cc}_{nm}^{\text{INT}} \simeq \text{cs}_{nm}^{\text{INT}} \simeq \text{sc}_{nm}^{\text{INT}} \simeq 0 \quad \text{for} \quad n \neq m \pm 1, \end{aligned} \quad (113)$$

where $n, m+1 \leq 3$ for $\text{INT} = \{1, 2\}$. For the unpolarized target, five nontrivial entries in the case of the unpolarized lepton beam appear, namely, $\text{cc}_{01,\text{unp}}^{\text{INT}}$, $\text{cc}_{10,\text{unp}}^{\text{INT}}$, $\text{cc}_{12,\text{unp}}^{\text{INT}}$, $\text{cc}_{21,\text{unp}}^{\text{INT}}$, and $\text{cc}_{32,\text{unp}}^{\text{INT}}$, which will be supplemented by three further Fourier coefficients in the polarized-beam case: $\text{cs}_{01,\text{unp}}^{\text{INT}}$, $\text{sc}_{10,\text{unp}}^{\text{INT}}$, and $\text{sc}_{21,\text{unp}}^{\text{INT}}$, while $\text{sc}_{12,\text{unp}}^{\text{INT}} \simeq \text{sc}_{32,\text{unp}}^{\text{INT}} \simeq 0$. To find their explicit form we have evaluated the products of Dirac bilinears. Again, for the unpolarized nucleon target we get

$$\begin{Bmatrix} \mathcal{S}_1 \\ \mathcal{S}_2 \end{Bmatrix}_{\mathcal{V}} = -4Q^2 \frac{(1-\eta)\eta}{y\tilde{y}\xi} \begin{Bmatrix} \tilde{y}K \cos \phi \\ y\tilde{K} \cos \varphi_\ell \end{Bmatrix} \mathcal{C}_{\mathcal{V},\text{unp}}(\mathcal{F}), \quad (114)$$

$$\begin{Bmatrix} \mathcal{R}_1 \\ \mathcal{R}_2 \end{Bmatrix}_{\mathcal{V}} = 4iQ^2 \frac{(1-\eta)\eta}{y\tilde{y}\xi} \begin{Bmatrix} \tilde{y}K \sin \phi \\ y\tilde{K} \sin \varphi_\ell \end{Bmatrix} \mathcal{C}_{\mathcal{V},\text{unp}}(\mathcal{F}), \quad (115)$$

$$\begin{Bmatrix} \mathcal{S}_1 \\ \mathcal{S}_2 \end{Bmatrix}_{\mathcal{A}} = -4iQ^2 \frac{(1-\eta)\eta}{y\tilde{y}\xi} \begin{Bmatrix} \tilde{y}K \sin \phi \\ y\tilde{K} \sin \varphi_\ell \end{Bmatrix} \mathcal{C}_{\mathcal{A},\text{unp}}(\mathcal{F}), \quad (116)$$

$$\begin{Bmatrix} \mathcal{R}_1 \\ \mathcal{R}_2 \end{Bmatrix}_{\mathcal{A}} = 4Q^2 \frac{(1-\eta)\eta}{y\tilde{y}\xi} \begin{Bmatrix} \tilde{y}K \cos \phi \\ y\tilde{K} \cos \varphi_\ell \end{Bmatrix} \mathcal{C}_{\mathcal{A},\text{unp}}(\mathcal{F}). \quad (117)$$

We introduced here universal electric- and magnetic-like combinations of the form factors intertwined with CFFs

$$\mathcal{C}_{\mathcal{V},\text{unp}} = F_1 \mathcal{H} - \frac{\Delta^2}{4M_N^2} F_2 \mathcal{E}, \quad \mathcal{C}_{\mathcal{A},\text{unp}} = -\eta(F_1 + F_2) \widetilde{\mathcal{H}}. \quad (118)$$

Then from Eqs. (80)–(86) and (98) the following nonzero Fourier coefficients for the first interference term are evaluated in a straightforward manner:

$$cc_{01,\text{unp}}^1 = -8\widetilde{K}(1-y)(2-y)(2-\tilde{y})\frac{\xi-\eta}{\eta}\Re\left\{\mathcal{C}_{\mathcal{V},\text{unp}}(\mathcal{F}) + \mathcal{C}_{\mathcal{A},\text{unp}}(\mathcal{F}) - \frac{\xi+\eta}{\xi}\mathcal{C}_{\mathcal{V},\text{unp}}(\mathcal{F}_L)\right\}, \quad (119)$$

$$cs_{01,\text{unp}}^1 = -8\lambda\widetilde{K}y(1-y)(2-\tilde{y})\frac{\xi-\eta}{\eta}\Im\left\{\mathcal{C}_{\mathcal{V},\text{unp}}(\mathcal{F}) + \mathcal{C}_{\mathcal{A},\text{unp}}(\mathcal{F}) + \frac{\xi+\eta}{\xi}\mathcal{C}_{\mathcal{V},\text{unp}}(\mathcal{F}_L)\right\}, \quad (120)$$

$$cc_{10,\text{unp}}^1 = 8K\Re\left\{(2-2y+y^2)(2-2\tilde{y}+\tilde{y}^2)\left(\frac{\xi}{\eta}\mathcal{C}_{\mathcal{V},\text{unp}}(\mathcal{F}) - \mathcal{C}_{\mathcal{A},\text{unp}}(\mathcal{F})\right) - 8(1-y)(1-\tilde{y})\frac{\xi^2-\eta^2}{\eta\xi}\mathcal{C}_{\mathcal{V},\text{unp}}(\mathcal{F}_L)\right\}, \quad (121)$$

$$cc_{12,\text{unp}}^1 = 16K(1-y)(1-\tilde{y})\frac{\xi+\eta}{\xi}\Re\left\{\mathcal{C}_{\mathcal{V},\text{unp}}(\mathcal{F}) + \mathcal{C}_{\mathcal{A},\text{unp}}(\mathcal{F})\right\}, \quad (122)$$

$$sc_{10,\text{unp}}^1 = -8\lambda K y(2-y)(2-2\tilde{y}+\tilde{y}^2)\Im\left\{\mathcal{C}_{\mathcal{V},\text{unp}}(\mathcal{F}) - \frac{\xi}{\eta}\mathcal{C}_{\mathcal{A},\text{unp}}(\mathcal{F})\right\}, \quad (123)$$

$$cc_{21,\text{unp}}^1 = -8\widetilde{K}(1-y)(2-y)(2-\tilde{y})\frac{\xi-\eta}{\eta}\Re\left\{\mathcal{C}_{\mathcal{V},\text{unp}}(\mathcal{F}) - \mathcal{C}_{\mathcal{A},\text{unp}}(\mathcal{F}) - \frac{\xi-\eta}{\xi}\mathcal{C}_{\mathcal{V},\text{unp}}(\mathcal{F}_L)\right\}, \quad (124)$$

$$sc_{21,\text{unp}}^1 = 8\lambda\widetilde{K}y(1-y)(2-\tilde{y})\frac{\xi-\eta}{\eta}\Im\left\{\mathcal{C}_{\mathcal{V},\text{unp}}(\mathcal{F}) - \mathcal{C}_{\mathcal{A},\text{unp}}(\mathcal{F}) + \frac{\xi-\eta}{\xi}\mathcal{C}_{\mathcal{V},\text{unp}}(\mathcal{F}_L)\right\}, \quad (125)$$

$$cc_{32,\text{unp}}^1 = 16K(1-y)(1-\tilde{y})\frac{\xi-\eta}{\eta}\Re\left\{\mathcal{C}_{\mathcal{V},\text{unp}}(\mathcal{F}) - \mathcal{C}_{\mathcal{A},\text{unp}}(\mathcal{F})\right\}, \quad (126)$$

supplemented by $ss_{12,\text{unp}}^1$, $ss_{21,\text{unp}}^1$, $cs_{21,\text{unp}}^1$, and $ss_{32,\text{unp}}^1$, which arise from Eq. (113). The corresponding expressions for the second interference term follow from Eqs. (87)–(93) and (98). For the unpolarized lepton beam they can be obtained from the symmetry under the exchange $k \leftrightarrow -\ell_-$ and $k' \leftrightarrow \ell_+$ as discussed above in section 4.1,

$$\left\{cc_{01}^2, cc_{10}^2, cc_{12}^2, cc_{21}^2, cc_{32}^2\right\}_{\text{unp}} = \left\{cc_{01}^1, cc_{10}^1, cc_{12}^1, cc_{21}^1, cc_{32}^1\right\}_{\text{unp}} \Big|_{\xi \rightarrow -\xi}^{y \leftrightarrow \tilde{y}}. \quad (127)$$

Here one has to keep in mind that $\mathcal{C}_{\mathcal{V}}$ and $\mathcal{C}_{\mathcal{A}}$ are even and odd functions in $\xi - i0$, respectively, and $\widetilde{K}(\xi, \tilde{y}) = K(-\xi, y = \tilde{y})$. It turns out that the remaining coefficients for the polarized lepton beam satisfy the following symmetry relations

$$\left\{cs_{01}^2, sc_{21}^2\right\}_{\text{unp}} = \sqrt{\frac{\tilde{y}-1}{1-y}} \left\{cs_{01}^1, sc_{21}^1\right\}_{\text{unp}} \Big|_{\xi \rightarrow -\xi}, \quad sc_{10,\text{unp}}^2 = -\sqrt{\frac{\tilde{y}-1}{1-y}} sc_{10,\text{unp}}^1 \Big|_{\xi \rightarrow -\xi}. \quad (128)$$

We note also that $\widetilde{K}(\xi, \tilde{y}) \approx \sqrt{(\tilde{y}-1)/(1-y)}K(-\xi, y)$. The explicit expressions of the Fourier coefficients for the second interference term are given in appendix B.2 together with the general structure and results for the polarized nucleon.

4.2.3 Squared Bethe-Heitler amplitude

The expressions for the Fourier coefficients of the pure BH term (99) are extremely lengthy and, therefore, will not be displayed here in an analytical form. In the following, we merely limit

ourselves to leading terms in the asymptotic expansion as $Q^2/\xi \rightarrow \infty$. Namely

$$\begin{aligned} \text{cc}_{00,\text{unp}}^{11} \approx & -2 \frac{1+\eta}{1-\eta} \left(1 - \frac{\xi}{\eta}\right) (1-y) \left\{ (2-2y+y^2)(2-2\tilde{y}+\tilde{y}^2) \left(1 + \frac{\xi^2}{\eta^2}\right) \right. \\ & \left. - 8(1-y)(1-\tilde{y}) \left(1 - \frac{\xi^2}{\eta^2}\right) \right\} \left\{ \left(1 - \frac{\Delta_{\min}^2}{\Delta^2}\right) \left(F_1^2 - \frac{\Delta^2}{4M^2} F_2^2\right) + \frac{2\eta^2}{1-\eta^2} (F_1 + F_2)^2 \right\}, \end{aligned} \quad (129)$$

$$\begin{aligned} \text{cc}_{02,\text{unp}}^{11} \approx & 2 \frac{1+\eta}{1-\eta} \left(1 - \frac{\xi}{\eta}\right) \left(1 - \frac{\xi^2}{\eta^2}\right) \left(1 - \frac{\Delta_{\min}^2}{\Delta^2}\right) (1-y) \left\{ (2-2y+y^2)(2-2\tilde{y}+\tilde{y}^2) \right. \\ & \left. + 8(1-y)(1-\tilde{y}) \right\} \left(F_1^2 - \frac{\Delta^2}{4M^2} F_2^2\right), \end{aligned} \quad (130)$$

$$\begin{aligned} \text{cc}_{11,\text{unp}}^{11} \approx & 4 \frac{1+\eta}{1-\eta} \left(1 - \frac{\xi}{\eta}\right) \frac{\sigma}{\eta} \sqrt{(1-y)(1-\tilde{y})(\xi^2 - \eta^2)} \\ & \times (1-y)(2-y)(2-\tilde{y}) \left\{ \left(1 + 3\frac{\xi}{\eta}\right) \left(1 - \frac{\Delta_{\min}^2}{\Delta^2}\right) \left(F_1^2 - \frac{\Delta^2}{4M^2} F_2^2\right) + \frac{4\xi\eta}{1-\eta^2} (F_1 + F_2)^2 \right\}, \end{aligned} \quad (131)$$

$$\begin{aligned} \text{cc}_{13,\text{unp}}^{11} \approx & -4 \frac{1+\eta}{1-\eta} \left(1 - \frac{\xi}{\eta}\right)^2 \left(1 - \frac{\Delta_{\min}^2}{\Delta^2}\right) \frac{\sigma}{\eta} \sqrt{(1-y)(1-\tilde{y})(\xi^2 - \eta^2)}, \\ & \times (1-y)(2-y)(2-\tilde{y}) \left(F_1^2 - \frac{\Delta^2}{4M^2} F_2^2\right), \end{aligned} \quad (132)$$

$$\text{cc}_{20,\text{unp}}^{11} \approx -4 \frac{1+\eta}{1-\eta} \left(1 + \frac{\xi}{\eta}\right) \left(1 - \frac{\xi^2}{\eta^2}\right) \left(1 - \frac{\Delta_{\min}^2}{\Delta^2}\right) (1-y)^2 (1-\tilde{y}) \left(F_1^2 - \frac{\Delta^2}{4M^2} F_2^2\right), \quad (133)$$

$$\begin{aligned} \text{cc}_{22,\text{unp}}^{11} \approx & 8 \frac{1+\eta}{1-\eta} \left(1 - \frac{\xi}{\eta}\right) \left(1 - \frac{\xi^2}{\eta^2}\right) (1-y)^2 (1-\tilde{y}) \\ & \times \left\{ \left(1 - \frac{\Delta_{\min}^2}{\Delta^2}\right) \left(F_1^2 - \frac{\Delta^2}{4M^2} F_2^2\right) + \frac{2\eta^2}{1-\eta^2} (F_1 + F_2)^2 \right\}, \end{aligned} \quad (134)$$

and the rest are expressed via the already known coefficients

$$\begin{aligned} \text{cc}_{24,\text{unp}}^{11} & \approx \frac{(\eta - \xi)^2}{(\eta + \xi)^2} \text{cc}_{20,\text{unp}}^{11}, & \text{ss}_{11,\text{unp}}^{11} & \approx \text{cc}_{11,\text{unp}}^{11} + 2 \frac{\eta + \xi}{\eta - \xi} \text{cc}_{13,\text{unp}}^{11}, \\ \text{ss}_{13,\text{unp}}^{11} & \approx \text{cc}_{13,\text{unp}}^{11}, & \text{ss}_{22,\text{unp}}^{11} & \approx \text{cc}_{22,\text{unp}}^{11}, & \text{ss}_{24,\text{unp}}^{11} & \approx \text{cc}_{24,\text{unp}}^{11}. \end{aligned} \quad (135)$$

One has to realize that this expansion is only valid if one stays away from kinematical boundaries, e.g., $y \ll 1$ is required. The reason for this is that the leading terms vanish with $(1-y)$ and subleading corrections become important as $y \rightarrow 1$. Contrary to the DVCS case, it appears that no partial cancellation occurs between the numerator and the denominator in the BH amplitude squared, so that in general the Fourier decomposition goes as high as up to the forth-order harmonics.

We note that the Fourier coefficients for the second BH-amplitude squared simply follow from the symmetry under $k \leftrightarrow -\ell_-$ and $k' \leftrightarrow \ell_+$. Since we extracted one power of ξ in front of the squared BH amplitude (99), we obtain the substitution rule

$$\text{cc}_{nm}^{22} = -\text{cc}_{nm}^{11} \Big|_{\xi \rightarrow -\xi}^{y \leftrightarrow \tilde{y}} \quad \text{and} \quad \text{ss}_{nm}^{22} = -\text{ss}_{nm}^{11} \Big|_{\xi \rightarrow -\xi}^{y \leftrightarrow \tilde{y}}, \quad (136)$$

while the remaining variables $\{\eta, \Delta^2, Q^2\}$ are kept unchanged. For the interference term of the first and second BH amplitudes the Fourier coefficients are

$$\text{cc}_{00,\text{unp}}^{12} \approx -8 \frac{1+\eta}{1-\eta} \frac{\xi}{\eta} \left(1 - \frac{\xi^2}{\eta^2}\right) (1-y)(2-y)(1-\tilde{y})(2-\tilde{y}) \quad (137)$$

$$\times \left\{ \left(1 - \frac{\Delta_{\min}^2}{\Delta^2}\right) \left(F_1^2 - \frac{\Delta^2}{4M^2} F_2^2\right) + \frac{2\eta^2}{1-\eta^2} (F_1 + F_2)^2 \right\},$$

$$\text{cc}_{02,\text{unp}}^{12} \approx 8 \frac{1+\eta}{1-\eta} \left(1 - \frac{\xi}{\eta}\right) \left(1 - \frac{\xi^2}{\eta^2}\right) (1-y)(2-y)(1-\tilde{y})(2-\tilde{y}) \left(1 - \frac{\Delta_{\min}^2}{\Delta^2}\right) \left(F_1^2 - \frac{\Delta^2}{4M^2} F_2^2\right), \quad (138)$$

$$\text{cc}_{11,\text{unp}}^{12} \approx -8 \frac{1+\eta}{1-\eta} \frac{\sigma}{\eta} \sqrt{(1-y)(1-\tilde{y})(\xi^2 - \eta^2)} \quad (139)$$

$$\times \left\{ (2-2y+y^2)(2-2\tilde{y}+\tilde{y}^2) \left[\frac{\xi^2}{\eta^2} \left(1 - \frac{\Delta_{\min}^2}{\Delta^2}\right) \left(F_1^2 - \frac{\Delta^2}{4M^2} F_2^2\right) + \frac{\xi^2 + \eta^2}{1-\eta^2} (F_1 + F_2)^2 \right] \right. \\ \left. - (1-y)(1-\tilde{y}) \left(1 - \frac{\xi^2}{\eta^2}\right) \left[9 \left(1 - \frac{\Delta_{\min}^2}{\Delta^2}\right) \left(F_1^2 - \frac{\Delta^2}{4M^2} F_2^2\right) + 10 \frac{\eta^2}{1-\eta^2} (F_1 + F_2)^2 \right] \right\},$$

$$\text{cc}_{20,\text{unp}}^{12} \approx -8 \frac{1+\eta}{1-\eta} \left(1 + \frac{\xi}{\eta}\right) \left(1 - \frac{\xi^2}{\eta^2}\right) \left(1 - \frac{\Delta_{\min}^2}{\Delta^2}\right) (1-y)(2-y)(1-\tilde{y})(2-\tilde{y}) \left(F_1^2 - \frac{\Delta^2}{4M^2} F_2^2\right), \quad (140)$$

$$\text{cc}_{22,\text{unp}}^{12} \approx -8 \frac{1+\eta}{1-\eta} \frac{\xi}{\eta} \left(1 - \frac{\xi^2}{\eta^2}\right) \quad (141)$$

$$\times (1-y)(2-y)(1-\tilde{y})(2-\tilde{y}) \left\{ \left(1 - \frac{\Delta_{\min}^2}{\Delta^2}\right) \left(F_1^2 - \frac{\Delta^2}{4M^2} F_2^2\right) + \frac{2\eta^2}{1-\eta^2} (F_1 + F_2)^2 \right\},$$

$$\text{ss}_{11,\text{unp}}^{12} \approx \text{cc}_{11,\text{unp}}^{12} - 8 \frac{1+\eta}{1-\eta} \frac{\sigma}{\eta} \sqrt{(1-y)(1-\tilde{y})(\xi^2 - \eta^2)} \left(1 - \frac{\xi^2}{\eta^2}\right) \quad (142)$$

$$\times \left\{ (2-2y+y^2)(2-2\tilde{y}+\tilde{y}^2) + 8(1-y)(1-\tilde{y}) \right\} \left(1 - \frac{\Delta_{\min}^2}{\Delta^2}\right) \left(F_1^2 - \frac{\Delta^2}{4M^2} F_2^2\right),$$

$$\text{ss}_{22,\text{unp}}^{12} \approx \text{cc}_{22,\text{unp}}^{12}. \quad (143)$$

Again, under the exchanges $k \leftrightarrow -\ell_-$ and $k' \leftrightarrow \ell_+$ both amplitudes are odd, i.e., $\mathcal{T}_{\text{BH}_1} \leftrightarrow -\mathcal{T}_{\text{BH}_2}$, and so their interference term is invariant. Thus, the Fourier coefficients must satisfy the relation

$$\text{cc}_{nm}^{12} = -\text{cc}_{mn}^{12} \Big|_{\xi \rightarrow -\xi}^{y \leftrightarrow \tilde{y}} \quad \text{and} \quad \text{ss}_{nm}^{12} = -\text{ss}_{mn}^{12} \Big|_{\xi \rightarrow -\xi}^{y \leftrightarrow \tilde{y}}, \quad (144)$$

which is the case for our result.

5 Measurements of GPDs

Having computed the cross section, we will discuss now the observables that can be used for the experimental exploration of GPDs.

5.1 Extraction of GPDs from electroproduction of electron pairs?

The major complication in the experimental measurement of the process is a rather small magnitude of the cross section which is suppressed by two powers of the electromagnetic coupling constant α_{em} compared to a typical deeply inelastic event. The other obstacle is the contamination of the heavy-photon events by the background of meson production. The latter can be circumvented in a relatively straightforward manner by avoiding the regions of $M_{\ell\bar{\ell}}^2$ close to meson-resonance thresholds. However, this certainly also restrict the phase space in the measurements of GPDs. For a general discussion of this issue we refer to Ref. [7]. We also note that a numerical estimate of this contamination can be done by means of Eqs. (51)-(52). Indeed, the contribution of the ρ meson resonance to the beam spin asymmetry turns out to be small in a perturbative QCD estimate [12].

Before turning to the discussion of possible measurements of GPDs in appropriate observables and presenting more quantitative estimates, we have to emphasize that a clear study of GPDs can be done in experiments in which the tagged flavor of the lepton pairs differs from the one of the beam. In case they are the same, the results deduced so far have to be supplemented by contributions in which the final electrons are interchanged. Under this exchange, the outgoing electron momenta jump places, i.e., $k' \leftrightarrow \ell_-$. This obviously yields an essentially different dependence of the VCS amplitude on the external variables. To employ the process with identical leptons for the extraction of information on GPDs, one has to ensure that the momentum flow in the quark propagator in the handbag diagram remains large. Indeed, the scalar product

$$p \cdot q' = -p \cdot q \frac{2 - y - y \cos \theta_\ell}{2y} \left\{ 1 + \mathcal{O} \left(\frac{\Delta_\perp}{\sqrt{p \cdot q}} \right) \right\}, \quad (145)$$

that sets the scale in the exchanged VCS amplitude remains large, however, it is now timelike. Note that here and in the following we denote the kinematical variables that enter the exchanged amplitudes with a prime. The power-suppressed contributions depend on all kinematical variables, especially, on y , \tilde{y} and both azimuthal angles ϕ and φ_ℓ . Besides $(2-y)/y > \cos \theta_\ell$, which is fulfilled by the usual kinematical restriction $y < 1$, no other *kinematical cuts* are required to ensure the applicability of perturbative QCD. Moreover, we find that η' is given by η in leading order

$$\eta' = \eta + \mathcal{O} \left(\frac{\Delta_\perp}{\sqrt{p \cdot q}} \right), \quad (146)$$

while ξ' receives a strong dependence on the leptonic variables:

$$\xi' = \xi \frac{2 \cos \theta_\ell - y(1 + \cos \theta_\ell)}{2 - y(1 + \cos \theta_\ell)} - \frac{2\sqrt{1-y}\sqrt{\eta^2 - \xi^2} \sin \theta_\ell}{2 - y(1 + \cos \theta_\ell)} \cos(\phi - \varphi_\ell) + \mathcal{O} \left(\frac{\Delta_\perp}{\sqrt{p \cdot q}} \right). \quad (147)$$

We point out that if θ_ℓ approaches the edge of phase space, i.e., $\theta_\ell \rightarrow \{0, \pi\}$, the absolute values of the scaling variables in Eq. (147) become identical $|\xi'| \simeq |\xi|$. The conclusions we draw from

our kinematical considerations are as follows. There are no crucial difficulties in the application of perturbative QCD as long as $p \cdot q$ is large, however, the analytical evaluation of observables and further studies are required to find an “optimal” method to deduce the (ξ, η) shape of GPDs from measurements of the reaction $e^\mp p \rightarrow e^\mp p e^+ e^-$.

5.2 Mapping the surface of GPDs

The most valuable information on GPDs can be accessed in observables that arise from the interference of the VCS and BH amplitudes, since they are proportional to linear combinations of the former. Such observables can be measured in single lepton- and hadron-spin asymmetries, in which the whole BH term squared drops out in the considered leading order in α_{em} , as well as in charge and angular asymmetries.

In the former case one accesses the imaginary part of the VCS amplitude, where the contamination of the squared VCS amplitude is expected to be small. Thus, to leading order accuracy in the QCD coupling α_s , see Eqs. (61) and (60), one measures the GPDs in the exclusive region. Schematically, we write

$$\frac{d\sigma^\uparrow - d\sigma^\downarrow}{d\sigma^\uparrow + d\sigma^\downarrow} \propto \sum_{\mathcal{F}=\mathcal{H} \dots \tilde{\mathcal{E}}_L} \mathcal{K}_{\mathcal{F}}(\phi, \varphi) \Im \mathcal{F}(\xi, \eta, \Delta^2), \quad (148)$$

where the imaginary part $\Im \mathcal{F}$ for $\tilde{\mathcal{H}}$ (\mathcal{H}) and $\tilde{\mathcal{E}}$ (\mathcal{E}) is a (anti)symmetric function of ξ (however, always symmetric in η)

$$\Im \mathcal{F} = \pi \sum_{q=u,d,s} Q_q^2 \left\{ F_q(\xi, \eta, \Delta^2) \mp F_q(-\xi, \eta, \Delta^2) \right\} + \mathcal{O}(\alpha_s). \quad (149)$$

The kinematical factors $\mathcal{K}_F(\phi, \varphi)$ can be read off from the Fourier coefficients, presented in section 4.2 and appendix B, where the squared BH amplitude, the scaled propagators \mathcal{P}_i and, at the edge of phase space, also the K and \tilde{K} factors should be exactly taken into account. In principle, a separation of different types of GPDs is partially feasible by a Fourier analysis or fully possible in case when single target-spin asymmetries are also available.

For the other two asymmetries, mentioned above, one uses the fact that the first (second) BH amplitude is even (odd) with respect to the interchange of both the lepton charge of the beam, i.e., $e^- \leftrightarrow e^+$, and the lepton’s momenta in the pair $\ell^- \leftrightarrow \ell^+$, i.e., with respect to the simultaneous replacement $\theta_\ell \rightarrow \pi - \theta_\ell$ and $\varphi_\ell \rightarrow \varphi_\ell + \pi$. On the other hand, the VCS amplitude is odd under charge and even under angular exchanges. A combination of both asymmetries offers the possibility to access the real part of the VCS amplitude without the contamination from the BH background. We point out that a certain separation of different types of Compton form factors can be done again by means of a Fourier analysis of unpolarized measurements, while the complete

separation requires double spin-flip experiments. Generically, these observables are analogous to the one in Eq. (148), where $\Im\mathcal{F}$ is replaced by the real part. To leading order in α_s , the real part of the Compton form factors is given by a “dispersion” relation:

$$\Re\mathcal{F}(\xi, \eta, \Delta^2) = \frac{1}{\pi} \text{PV} \int_{-1}^1 dx \frac{1}{\xi - x} \Im\mathcal{F}(x, \eta, \Delta^2) + \mathcal{O}(\alpha_s). \quad (150)$$

The value of this integral is also sensitive to the momentum fraction $|\eta| \leq |x|$, which is not probed in single spin asymmetries.

The unequal masses of the incoming and outgoing photons allow to probe GPDs away from the diagonal $|\xi| = |\eta|$, the only kinematics which is accessible in DVCS. The skewness variable η , given in Eq. (31), depends besides the photon energy $\omega_1 = \mathcal{Q}^2/2x_B M_N = yE$ (with respect to the target rest frame) mainly on the sum of both squared photon virtualities, i.e., $\mathcal{Q}^2 + M_{\ell\ell}^2$, while ξ essentially depends on their differences $\mathcal{Q}^2 - M_{\ell\ell}^2$. The boundaries of the (ξ, η) region, probed in the process, are set by the following kinematical constraints:

- The skewness parameter lies in the region $\eta_{\min} < \eta < 0$, where the lower bound comes from the kinematical condition $|\Delta^2| \geq |\Delta_{\min}^2|$:

$$-\eta_{\min} \leq \sqrt{-\Delta^2/(4M_N^2 - \Delta^2)}. \quad (151)$$

- The upper and lower value of ξ is a consequence of the quasi-real limit of the space- or timelike photon

$$-|\eta| < \xi < |\eta|. \quad (152)$$

- The minimal attained value of $|\xi| = 0$ stems from the condition $\mathcal{Q}^2 \simeq M_{\ell\ell}^2$.

In Fig. 6 it can be seen that the area of the surface probed in the electroproduction of the lepton pair is quite extensive. The three contours displayed in this figure embrace the areas to be probed for different values of the electron beam energy E , the lepton energy loss y , and the t -channel momentum transfer Δ^2 : (i) solid contour corresponds to $E = 11 \text{ GeV}$, $y = 0.5$, and $\Delta^2 = -0.3 \text{ GeV}^2$ ($M_N^2 \leq \mathcal{Q}^2 \leq 10 \text{ GeV}^2$), (ii) dashed contour corresponds to $E = 25 \text{ GeV}$, $y = 0.75$, and $\Delta^2 = -1 \text{ GeV}^2$ ($-4\Delta^2 \leq \mathcal{Q}^2 \leq 20 \text{ GeV}^2$), (iii) dotted contour corresponds to $E = 40 \text{ GeV}$, $y = 0.9$, and $\Delta^2 = -3 \text{ GeV}^2$ ($-4\Delta^2 \leq \mathcal{Q}^2 \leq 35 \text{ GeV}^2$). The corresponding values of the Bjorken variable are computed with the formula $x_B = \mathcal{Q}^2/(2M_N E y)$. It is obvious that the higher the energy of the lepton beam, the higher Δ^2 are allowed with observed applicability of the perturbative analysis of the Compton amplitude, and thus the higher values of $|\eta|$ are achieved.

We have addressed above only the case $\mathcal{Q}^2 > M_{\ell\ell}^2$ which probes $\xi > 0$ component of GPDs. For the reversed inequality, one gets information on the region $\xi < 0$ and probes patches of the two-dimensional surface analogous to the previous case. The positive mass of the final-state photon

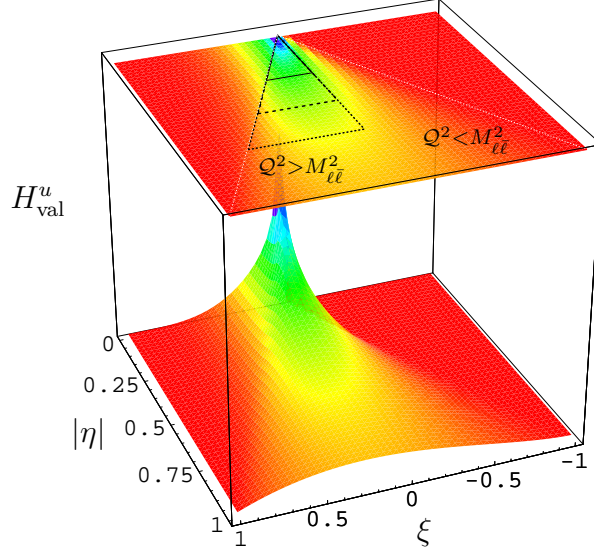


Figure 6: The coverage of the GPD surface (the valence component of the u -quark distribution, as an example) with electron beams of different energies: (solid contour) $E = 11$ GeV, (dashed contour) $E = 25$ GeV, (dotted contour) $E = 40$ GeV, as described in the text. [For simplicity, we discarded in this plot the change of the GPD with Δ^2 for different kinematical settings.]

allows to directly access only the exclusive, or distribution amplitude-like, component $|\eta| > |\xi|$ of the function. The inclusive, or parton distribution-like, component with $|\eta| < |\xi|$ requires spacelike virtuality for the outgoing photon which arises in two-photon exchange events in elastic electron-nucleon scattering. However, since the hadronic tensor (38) enters now via a loop integral, the single spin asymmetry measurements cannot be used for a direct extraction of GPDs.

5.3 Compton form factors

The magnitude of asymmetries depends on the relative strength of the BH amplitudes with respect to the VCS one. To get a rough idea of what happens we consider two limiting cases of the space- and timelike DVCS. In case of the production of a quasi-real final-state photon off the unpolarized proton target, the approximation of the amplitudes to leading power in Q^2 for $-\Delta_{\min}^2 \ll -\Delta^2 \ll 4M_N^2 \ll Q^2$ and $\xi \ll 1$ gives

$$\frac{|\mathcal{T}^{\text{DVCS}}|^2}{|\mathcal{T}^{\text{BH}}|^2} \sim \frac{1-y}{y^2} \frac{|\Delta^2|}{Q^2} \frac{\xi^2 |\mathcal{H}(\xi, \xi, \Delta^2)|^2}{F_1(\Delta^2)^2}, \quad (153)$$

for $M_{\ell\ell}^2 \rightarrow 0$ and large Q^2 . One expects that $|\mathcal{H}(\xi, \xi, \Delta^2)|$ behaves like ξ^{-1} and, thus, the ratio (153) is essentially $(1-y)|\Delta^2|/y^2 Q^2$. Obviously, the kinematical suppression by $|\Delta^2|/Q^2$ can be removed in the small- y region and, therefore, the DVCS cross section can be extracted in collider

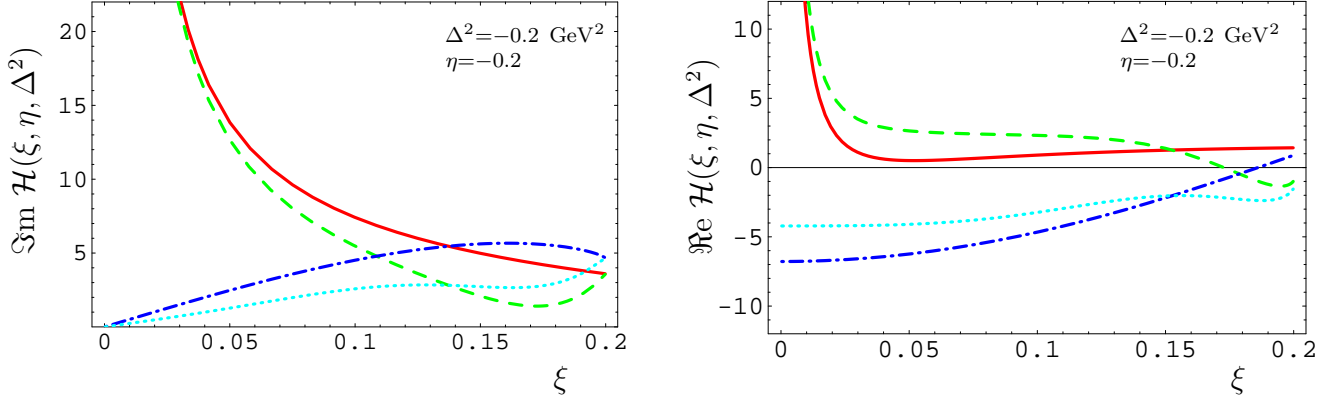


Figure 7: The imaginary and real part of $\mathcal{H}(\xi, \eta = -0.2, \Delta^2 = -0.2 \text{ GeV}^2)$ plotted versus ξ in the left and right panel, respectively, for different GPD models: $b^{\text{val}} = b^{\text{sea}} = \infty$ and $B^{\text{sea}} = 5 \text{ GeV}^{-2}$ (solid, dashed) as well as for $b^{\text{val}} = b^{\text{sea}} = 1$ and $B^{\text{sea}} = 9 \text{ GeV}^{-2}$ (dash-dotted, dotted) with (dashed, dotted) and without (solid, dotted) D -term.

experiments. On the other hand, for moderate values of y , one finds a rather sizeable (beam-spin) asymmetries in fixed target experiments. In contrast, in case of the timelike DVCS, replacing the variables $y \rightarrow \tilde{y}$ and $Q^2 \rightarrow -M_{\ell\bar{\ell}}^2$ in the above equation, we find the ratio

$$\frac{|\mathcal{T}^{\text{DVCS}}|^2}{|\mathcal{T}^{\text{BH}}|^2} \sim \frac{\sin^2 \theta_\ell}{4} \frac{|\Delta^2|}{M_{\ell\bar{\ell}}^2} \frac{\xi^2 |\mathcal{H}(\xi, \xi, \Delta^2)|^2}{F_1(\Delta^2)^2}, \quad (154)$$

for $Q^2 \rightarrow 0$ and large $M_{\ell\bar{\ell}}^2$. It is always suppressed by $1/M_{\ell\bar{\ell}}^2$ and so the BH cross section overwhelms the VCS ones [10]. Thus, one anticipates that the second BH amplitude dominates the cross section except when one approaches the limit $M_{\ell\bar{\ell}} \rightarrow 0$. On this basis one would naively argue that the asymmetries will be suppressed as well. To get rid partly of this problem, instead of integrating over the full range of the lepton-pair scattering angles, one rather has to sum over a restricted domain and exclude the endpoint regions $\theta_\ell = \{0, \pi\}$.

To give quantitative estimates and provide some insights into the procedure of extracting GPDs from such experiments, we use several GPD models with quite distinct behavior in the central region. For the GPDs H_q , where q labels the three light (anti-)quarks, we take the factorized version of the (ξ, η) and Δ^2 dependence, i.e., $H_q(\xi, \eta, \Delta^2) = F_q(\Delta^2)H_q(\xi, \eta, \Delta^2 = 0)$, where the reduced GPD at zero momentum $\Delta^2 = 0$ is modeled via a factorized double distribution (DD) ansatz [15]. For specific details we refer the reader to Ref. [9]. The essential freedom left within this specification concerns the parameter b^q of the profile function, which controls the strength of the η -dependence of the reduced GPDs $H_q(\xi, \eta, \Delta^2 = 0)$, the slope of the partonic sea form factor,

$$F^{\text{sea}}(\Delta^2) = \left(1 - \frac{B^{\text{sea}}}{3}\Delta^2\right)^{-3}, \quad (155)$$

and the D -term⁴, given as an expansion in terms of Gegenbauer polynomials [31]

$$D(\xi, \eta, \Delta^2) = \frac{\theta(|\xi| \leq |\eta|) \text{sign}(\eta)}{(1 - \Delta^2/0.77 \text{GeV}^2)^3} (1 - x^2) \left(-4C_1^{3/2}(x) - 1.2C_3^{3/2}(x) - 0.4C_5^{3/2}(x) \right) \Big|_{x=\frac{\xi}{\eta}}. \quad (156)$$

The latter is entirely concentrated in the central region $|\xi| \leq |\eta|$. The imaginary and real parts of the Compton form factors for these models are shown in Fig. 7. In case the skewness effect is eliminated (as $b \rightarrow \infty$), we model the reduced GPDs by the usual forward parton densities taken in MRS A' parameterization at the input scale $\mu^2 = 4 \text{ GeV}^2$. Consequently, for this so-called FPD-model the imaginary and real parts strongly increase as ξ gets smaller. This is displayed by the solid and dashed lines in Fig. 7. On the contrary, for $b = 1$, — for brevity we call this choice as the DD-model, — (dash-dotted and dotted lines), the contribution in the central region is suppressed and goes to zero for the imaginary part when $\xi \rightarrow 0$. At the same time, the real part approaches a constant, with the value determined by the inverse moment of GPDs

$$\Re \mathcal{H}(\xi = 0, \eta, \Delta^2) = - \int_{-1}^1 \frac{dx}{x} \sum_{q=u,d,s} Q_q^2 \{ H_q(x, \eta, \Delta^2) - H_q(-x, \eta, \Delta^2) \}. \quad (157)$$

The amplitudes supplemented by the D -term contributions are presented by the dashed and dotted lines in Fig. 7. It is clearly demonstrated that their effect is especially prominent (within the parameter range chosen for the estimates) in the real part of the Compton form factors where it changes their sign in the vicinity of $\xi \rightarrow \pm\eta$.

5.4 Single-spin asymmetries

Now, having discussed the properties of the Compton form factors, we will have a closer look on single-spin asymmetries, in particularly, the beam-spin asymmetry for the proton

$$d\sigma^\uparrow - d\sigma^\downarrow \propto (\pm \mathcal{T}_{\text{BH}_1}^* + \mathcal{T}_{\text{BH}_2}^*) \Im \mathcal{T}_{\text{VCS}} + \dots. \quad (158)$$

Potentially, the interference term could be contaminated by the imaginary part $\Im \mathcal{T}_{\text{VCS}} \mathcal{T}_{\text{VCS}}^\dagger$, arising from the interference of twist-two and -three Compton form factors. As for the DVCS process [9] we expect, assuming the smallness of three-particle correlations, that this contribution can be safely neglected. As mentioned above, in leading order of perturbation theory, the single spin asymmetries are directly proportional to the linear combination of GPDs $\sum_{q=u,d,s} Q_q^2 \{ F_q(\xi, \eta, \Delta^2) \mp F_q(\xi, -\eta, \Delta^2) \}$, where $(+)$ — applies for (axial-) vector-type GPDs. For instance, eight leading-twist observables are measurable in the beam-spin asymmetry, which are

⁴Note that this D -term, taken from the quark soliton model [29, 30] at a low scale $\mu \sim 0.6 \text{ GeV}$, will mix under scale evolution with a gluonic D -term. For the present considerations it is suffice to neglect the scale dependence completely.

coming in pairs from the interference of the VCS with the first and second BH amplitudes⁵: cs_{01}^1 , sc_{10}^1 , sc_{21}^1 , cs_{12}^1 as well as cs_{01}^2 , sc_{10}^2 , sc_{21}^2 , cs_{12}^2 , see Eq. (128). However, they depend only on two different linear combinations (118) of GPDs:

$$F_1(\mathcal{H} + \mathcal{H}_L) - \frac{\Delta^2}{4M_N^2} F_2(\mathcal{E} + \mathcal{E}_L), \quad -\eta(F_1 + F_2)\widetilde{\mathcal{H}} + \frac{\eta}{\xi} \left(F_1 \mathcal{H}_L - \frac{\Delta^2}{4M_N^2} F_2 \mathcal{E}_L \right). \quad (159)$$

Consequently, there there exist six constraints among the whole set of coefficients, which can be expressed as:

$$\begin{aligned} sc_{10}^1 &\simeq -\frac{(2-y)(2-2\tilde{y}+\tilde{y}^2)}{2(1-y)(2-\tilde{y})} \frac{\sqrt{(1-y)(\xi-\eta)}}{\sqrt{(1-\tilde{y})(\xi+\eta)}} \left\{ cs_{01}^1 + \frac{\xi+\eta}{\xi-\eta} sc_{21}^1 \right\}, \\ \frac{cs_{01}^2}{sc_{21}^1} &\simeq \frac{sc_{10}^2}{sc_{10}^1} \simeq \frac{sc_{21}^2}{cs_{01}^1} \simeq -\frac{\sqrt{(1-\tilde{y})(\xi+\eta)}}{\sqrt{(1-y)(\xi-\eta)}}, \end{aligned} \quad (160)$$

supplemented by the relation (113), i.e., $cs_{21}^1 \simeq -sc_{21}^1$ and $cs_{21}^2 \simeq -sc_{21}^2$. Another consequence of Eq. (159) is that the beam-spin asymmetry gives us no handle on the Callan-Gross relation, i.e., the longitudinal Compton form factors can not be separated from the leading ones. The Fourier coefficients are projected out by taking the following moments, when integrated over the scattering and azimuthal angles:

$$\begin{aligned} \sin \phi &\rightarrow sc_{10}^1, \quad \cos \theta_\ell \sin \varphi_\ell \rightarrow cs_{01}^1, \quad \cos \theta_\ell \cos \varphi_\ell \sin(2\phi) \rightarrow sc_{21}^1, \quad \cos \theta_\ell \sin \varphi_\ell \cos(2\phi) \rightarrow cs_{21}^1, \\ \sin \phi_\ell &\rightarrow sc_{10}^2, \quad \cos \theta_\ell \sin \phi \rightarrow cs_{01}^2, \quad \cos \theta_\ell \sin(2\varphi_\ell) \cos \phi \rightarrow sc_{21}^2, \quad \cos \theta_\ell \cos(2\varphi_\ell) \sin \phi \rightarrow cs_{21}^2, \end{aligned}$$

where the weight in the first (second) row is even (odd) under the reflection $\theta_\ell \rightarrow \pi - \theta_\ell$ and $\varphi_\ell \rightarrow \pi + \varphi_\ell$. In the same line of thinking, one can study the Fourier coefficients for the single target-spin asymmetries. Because of the substitution rules (B.34) and (B.35), the number of the Compton form factors will be the same as for the case of charge and angular asymmetries, discussed below. Of course, single target-spin asymmetries are given by the imaginary part of new linear combinations in GPDs with a characteristic angular dependence.

As we conclude from Eq. (160), the same information on GPDs is obtained by taking the appropriate moments in ϕ or φ_ℓ . However, the size of the complementary beam-spin asymmetries can vary. Moreover, if one takes the asymmetry from the interference with the second BH amplitude, the weight must be odd and, thus, we have no contamination from the squared VCS amplitude. To suppress the squared BH amplitude, we integrate over the region $\pi/4 \leq \theta_\ell \leq 3\pi/4$ and form alternatively the $\sin \phi$ or $\sin \varphi_\ell$ moments. This picks up the coefficients sc_{10}^1 and sc_{10}^2 ,

⁵For brevity we neglect throughout this section in the Fourier coefficients the subscript “unp”, which refers to the unpolarized target.

respectively, cf. Eqs. (98), (100), and (113). Thus, the beam-spin asymmetry

$$\begin{aligned} \left\{ \begin{array}{c} A_{\text{LU}}^{\sin \phi} \\ A_{\text{LU}}^{\sin \varphi_\ell} \end{array} \right\} &= \frac{1}{\mathcal{N}} \int_{\pi/4}^{3\pi/4} d\theta_\ell \int_0^{2\pi} d\varphi_\ell \int_0^{2\pi} d\phi \left\{ \begin{array}{c} 2 \sin \phi \\ 2 \sin \varphi_\ell \end{array} \right\} \frac{d\sigma^\uparrow - d\sigma^\downarrow}{d\Omega_\ell d\phi} \\ &\propto \Im \left\{ F_1 \mathcal{H} - \frac{\Delta^2}{4M_N^2} F_2 \mathcal{E} + \xi (F_1 + F_2) \widetilde{\mathcal{H}} \right\}, \end{aligned} \quad (161)$$

with the normalization factor being

$$\mathcal{N} = \int_{\pi/4}^{3\pi/4} d\theta_\ell \int_0^{2\pi} d\varphi_\ell \int_0^{2\pi} d\phi \frac{d\sigma^\uparrow + d\sigma^\downarrow}{d\Omega_\ell d\phi},$$

is analogous to the one defined in the case of space- and timelike DVCS. For the proton target it is mainly sensitive to the contribution $F_1 \Im \mathcal{H}$ and, therefore, we might neglect in our estimate the other two Compton form factors.

In Fig. 8, we show the beam-spin asymmetries (161) for an 11 GeV electron beam and $\eta = -0.2$, $\Delta^2 = -0.2 \text{ GeV}^2$ ($\Delta_{\text{min}}^2 \approx -0.15 \text{ GeV}^2$), and $y = 0.5$. We fix the value of $\mathcal{Q}^2 + \mathcal{M}_{\ell\bar{\ell}}^2 \approx 3.4 \text{ GeV}^2$, i.e., $Q^2/\xi \approx 8.5 \text{ GeV}^2$, and scan the $-0.2 < \xi < 0.2$ region by varying the virtuality Q^2 in the range $0 \leq Q^2 \leq 3.4 \text{ GeV}^2$. In the spacelike DVCS limit (the left panel with $\xi \rightarrow -\eta$, $x_B \approx 0.33$), we uncover a typical beam-spin asymmetry of order 20% measured in fixed target experiments. This asymmetry is getting smaller in the DD-model (dashed and dash-dotted line) with increasing ξ , reflecting the fact that the imaginary part of the Compton form factor goes to zero (see Fig. 7). We stress that this feature truly arises from the GPD model, since ξ/Q^2 is fixed and so no essential kinematical suppression of the interference term arises as $\xi \rightarrow 0$. The negative D -term slightly changes the normalization away from the edges of phase spaces. In case of the FPD-model, the interference term increases at $\xi \rightarrow 0$ with $\xi^{-1-\lambda}$ (for MRS A' parametrization $\lambda = 0.17$), as a consequence of the small- x behavior of the sea-quark densities. On the other hand, the VCS cross section in the denominator increases like $\xi^{-2-2\lambda}$, overwhelming the BH contributions, and forces the asymmetry to vanish at $\xi = 0$. This explains why with the FPD-model the asymmetry remains sizeable over a large interval of ξ . The asymmetry, formed with $\sin \phi$ is considerably smaller in the timelike region, compared with the spacelike one, since the first BH amplitude, responsible for this asymmetry, is getting smaller, while the second BH amplitude, entering the denominator, increases for $\xi \rightarrow -|\eta|$. Forming the moments with respect to the $\sin \varphi_\ell$ (the right panel of Fig. 8), the asymmetry is caused by the interference with the second BH amplitude. As explained above, we expect that this amplitude is in general larger than the first one and results into a rather sizeable asymmetry not only in the time- but also in the spacelike region.

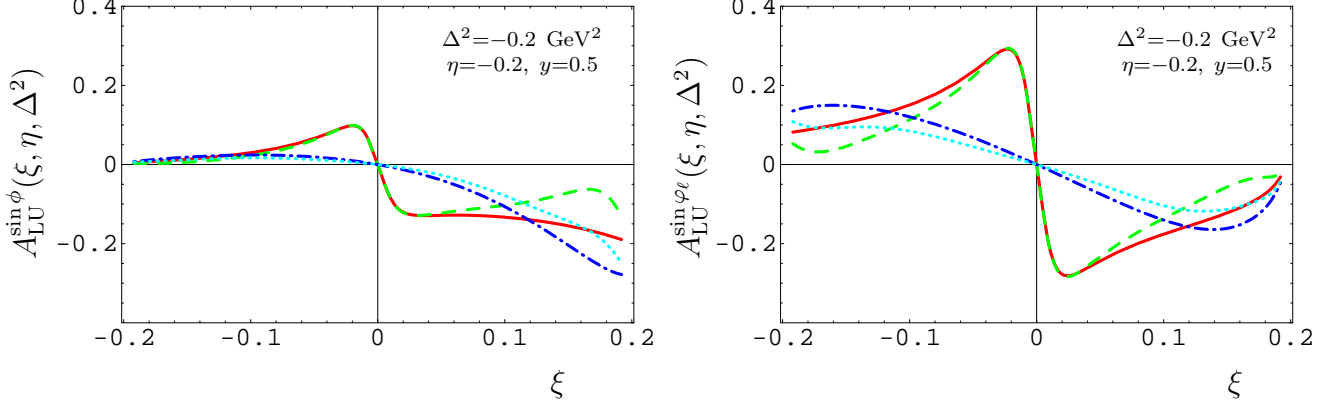


Figure 8: Beam spin asymmetries of $A_{\text{LU}}^{\sin \phi}$ and $A_{\text{LU}}^{\sin \phi_\ell}$ as functions of ξ , respectively, for $\eta = -0.2$, $\Delta^2 = -0.2 \text{ GeV}^2$, $y = 0.5$ and different GPD models, specified in Fig. 7.

5.5 Charge and angular asymmetries

Let us now comment on charge and angular asymmetries, in which the Fourier coefficients cc_{01}^1 , cc_{10}^1 , $cc_{12}^1 \simeq ss_{12}^1$, $cc_{21}^1 \simeq ss_{21}^1$, and $cc_{32}^1 \simeq ss_{32}^1$ as well as the complementary set of the second interference term are attainable. As above, the Fourier coefficients of both interference terms are related by

$$\frac{cc_{01}^2}{cc_{21}^1} \simeq \frac{cc_{10}^2}{cc_{10}^1} \simeq \frac{cc_{12}^2}{cc_{32}^1} \simeq \frac{cc_{21}^2}{cc_{01}^1} \simeq \frac{cc_{32}^2}{cc_{12}^1} \simeq -\frac{\sqrt{(1-\tilde{y})(\xi+\eta)}}{\sqrt{(1-y)(\xi-\eta)}}. \quad (162)$$

There are now three independent Compton form factors $\mathcal{C}_{\mathcal{V},\text{unp}}(\mathcal{F})$, $\mathcal{C}_{\mathcal{V},\text{unp}}(\mathcal{F}_L)$, and $\mathcal{C}_{\mathcal{A},\text{unp}}(\mathcal{F})$, given in Eq. (118), which can be accessed there. Consequently, there exist two constraints among five nontrivial Fourier coefficients. Provided the Callan-Gross relation is assumed to be fulfilled, this number increases to three:

$$\begin{aligned} cc_{10}^1 &\simeq -\frac{(2-2y+y^2)(2-2\tilde{y}+\tilde{y}^2)}{2(2-y)(1-\tilde{y})(2-\tilde{y})} \frac{\sqrt{(1-\tilde{y})(\xi+\eta)}}{\sqrt{(1-y)(\xi-\eta)}} \left\{ \frac{\xi-\eta}{\xi+\eta} cc_{01}^1 + cc_{21}^1 \right\}, \\ cc_{12}^1 &\simeq \frac{-2(1-y)}{(2-y)(2-\tilde{y})} \frac{\sqrt{(1-\tilde{y})(\xi+\eta)}}{\sqrt{(1-y)(\xi-\eta)}} cc_{01}^1, \\ cc_{32}^1 &\simeq \frac{-2(1-\tilde{y})}{(2-y)(2-\tilde{y})} \frac{\sqrt{(1-y)(\xi-\eta)}}{\sqrt{(1-\tilde{y})(\xi+\eta)}} cc_{21}^1. \end{aligned} \quad (163)$$

We add that charge and angular asymmetries can be combined with double spin-flip experiments, which offer information on a new combination of GPDs. As in the case of the beam-spin asymmetry, the number of independent Compton form factors is, however, reduced to two, as a consequence of our results (B.34) and (B.35).

The charge odd part is given by the interference of the first BH amplitude with the VCS as well as with the second BH ones. For unpolarized settings the charge asymmetry reads

$$d\sigma^+ - d\sigma^- \propto \mathcal{T}_{\text{BH}_1}^* \mathcal{T}_{\text{BH}_2} + \Re \left(\mathcal{T}_{\text{BH}_1}^* \mathcal{T}_{\text{VCS}} \right). \quad (164)$$

Taking now moments with respect to the solid angle of the final state that are even under reflection, e.g., by means of the weight function

$$w^{\text{even}}(\phi_\ell, \theta_\ell) = \{1, \cos \phi_\ell \cos \theta_\ell, \cos(2\phi_\ell), \sin \phi_\ell \cos \theta_\ell, \sin(2\phi_\ell), \dots\}, \quad (165)$$

the contamination of the BH interferences drops out:

$$\int d\Omega_\ell w^{\text{even}}(\phi_\ell, \theta_\ell) \frac{d\sigma^+ - d\sigma^-}{d\Omega_\ell} \propto \int d\Omega_\ell w^{\text{even}}(\phi_\ell, \theta_\ell) \Re \left(\mathcal{T}_{\text{BH}_1}^* \mathcal{T}_{\text{VCS}} \right). \quad (166)$$

Corresponding to the choice of the weight function, this average will provide Fourier series in ϕ , where the zeroth, first, second and third harmonics lead to access to all leading-twist coefficients of the first interference term. In case when only the lepton beam of a specified single charge is available, one can form asymmetries with an odd weight

$$\begin{aligned} w^{\text{odd}}(\phi_\ell, \theta_\ell) \\ = \{ \cos \theta_\ell, \cos \varphi_\ell, \cos(2\varphi_\ell) \cos \theta_\ell, \cos(3\varphi_\ell), \sin \varphi_\ell, \sin(2\varphi_\ell) \cos \theta_\ell, \sin(3\varphi_\ell), \dots \}, \end{aligned} \quad (167)$$

so that the squared amplitudes exactly drop out

$$\int d\Omega_\ell w^{\text{odd}}(\phi_\ell, \theta_\ell) \frac{d\sigma}{d\Omega_\ell} \propto \int d\Omega_\ell w^{\text{odd}}(\phi_\ell, \theta_\ell) \left\{ \pm \mathcal{T}_{\text{BH}_1}^* \mathcal{T}_{\text{BH}_2} + \Re \left(\mathcal{T}_{\text{BH}_2}^* \mathcal{T}_{\text{VCS}} \right) \right\}. \quad (168)$$

After the subtraction of the remaining BH interference is done, one measures the leading twist-two Fourier coefficients. Still, this procedure may allow a handle on the real part of the Compton form factors. If both kinds of the lepton-beam charges are available, the BH contribution drops in the charge even combination

$$\int d\Omega_\ell w^{\text{odd}}(\phi_\ell, \theta_\ell) \frac{d\sigma^+ + d\sigma^-}{d\Omega_\ell} \propto \int d\Omega_\ell w^{\text{odd}}(\phi_\ell, \theta_\ell) \Re \left(\mathcal{T}_{\text{BH}_2}^* \mathcal{T}_{\text{VCS}} \right). \quad (169)$$

To illustrate the feasibility of the subtraction procedure, we consider the charge and the angular asymmetries

$$\left\{ \frac{A_{\text{CA}}^{\cos \varphi_\ell}}{A^{\cos \varphi_\ell}} \right\} = \frac{1}{\mathcal{N}} \int_{\pi/4}^{3\pi/4} d\theta_\ell \int_0^{2\pi} d\phi \int_0^{2\pi} d\varphi_\ell 2 \cos \varphi_\ell \left\{ \frac{(d\sigma^+ + d\sigma^-)/2d\Omega_\ell d\phi}{d\sigma^-/d\Omega_\ell d\phi} \right\}, \quad (170)$$

performed with respect to $2 \cos \varphi_\ell$, where in both cases we choose the normalization to be

$$\mathcal{N} = \int_{\pi/4}^{3\pi/4} d\theta_\ell \int_0^{2\pi} d\phi \int_0^{2\pi} d\varphi_\ell \frac{d\sigma^-}{d\Omega_\ell d\phi}.$$

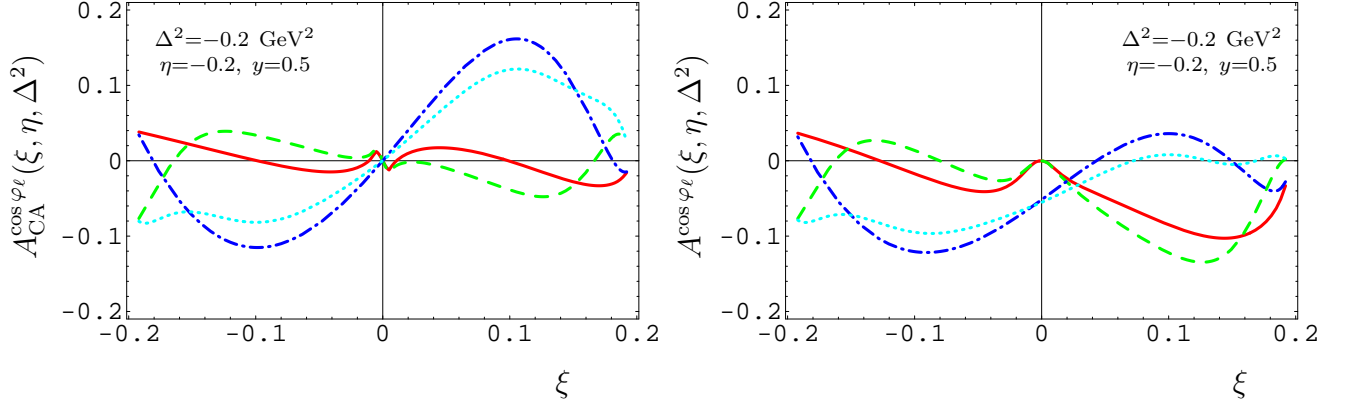


Figure 9: The charge asymmetry $A_{CA}^{\cos \varphi_\ell}$ and angular asymmetry $A^{\cos \varphi_\ell}$ are displayed versus ξ in the left and right panel, respectively, for the same kinematics as in Fig. 8 and different GPD models, specified in Fig. 7.

These asymmetries project the Fourier coefficient cc_{10}^2 of the second BH-VCS interference term, which is, in the absence of \mathcal{F}_L , proportional to

$$cc_{10}^2 \propto \Re \left\{ \frac{\xi}{\eta} F_1 \mathcal{H} - \frac{\xi}{\eta} \frac{\Delta^2}{4M_N^2} F_2 \mathcal{E} + \eta (F_1 + F_2) \widetilde{\mathcal{H}} \right\}, \quad (171)$$

making use of Eq. (B.28). One realizes that \mathcal{H} is now suppressed by a factor ξ/η and, thus, with decreasing $|\xi|$ the contribution of $\widetilde{\mathcal{H}}$ starts to be important. However, for the sake of simplicity, we will set $\widetilde{\mathcal{H}}$ for the illustration purposes to zero. In Fig. 9 we display these asymmetries in two different panels for the same kinematics and GPD models as employed above for spin asymmetries. Clearly, the shape of these asymmetries is in any case dictated by the GPD models. The left panel shows the charge asymmetry. One realizes, that as in Fig. (7), the D -term is responsible for the sign change of the asymmetries⁶, when ξ approaches $\mp\eta$: compare solid (dash-dotted) with dashed (dotted) line. The size of the asymmetries in the range $-|\eta| < \xi < |\eta|$ is driven by the parameterization of the reduced GPD, see also Fig. 7. We observe that in the timelike region ($\xi < 0$) both asymmetries are rather similar, while in the spacelike region the angular asymmetry, compared to the charge asymmetry, is shifted downwards. This is caused by the interference of both BH amplitudes, where the first one becomes small, compared to the VCS amplitude, in the timelike region. Due to the additional power of ξ , indicated in Eq. (171), the charge asymmetry with the DD-model goes to zero at $\xi \rightarrow 0$. This features will not be changed, if one includes $\widetilde{\mathcal{H}}$, since its real part is antisymmetric in ξ . For the FPD-model both asymmetries go to zero which is caused by the fact that the normalization \mathcal{N} as in the case of beam-spin asymmetries strongly

⁶We remind the known fact, that for $\xi = \eta$ there is a competition in sign between the regular valence and sea quark GPDs. The resulting sign at $\xi = \pm\eta$ is a consequence of chosen parametrizations, and can not be taken as a clear-cut signature for the D -term contribution.

increase for $\xi \rightarrow 0$. We note that the wiggles around the point $\xi \rightarrow 0$ of the solid and dashed line in the left panel arise from the competition in the numerical increase of the numerator and denominator.

We remark that as in the case of DVCS charge and angular asymmetries might be contaminated stronger by twist-three effects than the beam-spin asymmetries. They are mainly of kinematical origin, i.e., expressed by twist-two GPDs and generate Fourier coefficients cc_{00}^{INT} , $ss_{11}^{\text{INT}} \simeq cc_{11}^{\text{INT}}$, and $ss_{22}^{\text{INT}} \simeq cc_{22}^{\text{INT}}$ that do not necessarily vanish at the kinematical boundaries.

5.6 Collider experiments

Finally, we address the question of whether GPDs can also be measured in the small- η region with lepton-hadron collider experiments. Analogously to the above Eqs. (153) and (154) one can estimate the ratio of the BH and VCS cross sections by

$$\begin{aligned} \frac{\int d\varphi_\ell \int d\phi |\mathcal{T}^{\text{VCS}}|^2}{\int d\varphi_\ell \int d\phi |\mathcal{T}^{\text{BH}}|^2} &\sim \frac{2\eta^2 |\Delta^2|}{(\xi^2 + \eta^2)(\mathcal{Q}^2 + \mathcal{M}_{\ell\bar{\ell}}^2)} \\ &\times \frac{2\eta(1-y)\sin^2\theta_\ell}{4(\xi+\eta)(1-y) - y^2(\xi-\eta)\sin^2\theta_\ell} \frac{\eta^2 |\mathcal{H}(\xi, \eta, \Delta^2)|^2 (1 + \dots)}{F_1(\Delta^2)^2 (1 + \dots)}. \end{aligned} \quad (172)$$

Here the ellipses stand for the ratio of terms that arise solely from the scattering by longitudinally and transversely polarized photons. They vanish in the DVCS limits and will be omitted since they do not affect our qualitative considerations. The first kinematical factor, essentially equal to $|\Delta^2|/(\mathcal{Q}^2 + \mathcal{M}_{\ell\bar{\ell}}^2)$, should be much smaller than one to ensure the applicability of perturbative QCD. The second term is, over a wide kinematical range, (much) smaller than one, except when one approaches the spacelike DVCS limit. In this case it goes like $1/y^2$ and gives the desired kinematical enhancement, which allows to measure the DVCS cross section at small value of y . Staying away from this limit we already see that the VCS cross section is kinematically suppressed by at least one order of magnitude, or so, compared to the BH one. Of course, the behavior of $\eta\mathcal{H}(\xi, \eta, \Delta^2)$ is completely unknown in the central region, since it has never been measured so far. Theoretically, we are facing here new non-perturbative phenomena for which the connection to forward parton densities is lost. So there is a lot of space for speculations, which should be clarified by experimental measurements. If we take the FPD-model, then $\mathcal{H}(\xi, \eta, \Delta^2)$ grows like $\xi^{-1-\lambda}$ as ξ goes to zero. Certainly, the kinematical suppression will be overwhelmed by this rise in the equal mass limit, $\mathcal{Q}^2 \simeq M_{\ell\bar{\ell}}^2$. We have found no plausible arguments of why this should happen. We note, that if the sea-quark GPD does not vanish at $\xi = 0$ as $x = 0$, the real part of the Compton form factor will blow up. In case the GPD is vanishing at this particular point, we still expect that the real part, given by the integral (157) over the whole x range, goes with $\#\eta^{-1-\lambda}$, which follows from rather general considerations based on the DD-representation of GPDs and

the fact that they have to reduce to the parton densities in the kinematical forward limit. The available DVCS measurements, analyzed with leading order formulas of perturbative QCD, tell us that the sea-quark GPD is rather sizeable at the point $\xi = -\eta$. Consequently, there is only a small amount of the phase-space left, in which the GPD goes to zero at $x = 0$. The way this happens will be essentially up to the prefactor $\#$, we do not know. We conclude, that the only chance to have an experimental handle on the VCS cross section is in the kinematical region in which Δ^2 is small, $\mathcal{Q}^2 + \mathcal{M}_{\ell\bar{\ell}}^2$ should be several times larger than the average $\langle\langle -\Delta^2 \rangle\rangle$ and at least one or two GeV^2 and y should rather large to ensure that $|\eta|$ is small. For instance, in the case of H1 and ZEUS experiments we find for $y = 0.5$, $\eta = -2.2 \times 10^{-5}$, $\langle\langle \Delta^2 \rangle\rangle = -0.1 \text{ GeV}^2$ and $\theta_\ell = \pi/4$ within the DD model that the ratio (172) is of order one for a large interval of $-|\eta|/2 < \xi \leq |\eta|$. Similar estimates can be done for the charge and angular asymmetries, where one should project the Fourier coefficient c_{01}^2 , which, compared to c_{10}^2 , is not plagued from an additional suppression factor ξ/η .

6 Conclusions

In the present paper we have studied the process $eN \rightarrow e'N'\ell\bar{\ell}$. We have elaborated the structure of the cross section to leading power in the hard momentum. The power suppressed twist-three contributions, though have not been discussed presently, generate further harmonics in the squared amplitude. For instance, they induce the off-diagonal elements in the coefficient matrix of the squared VCS amplitude, e.g., cc_{nm} with $n \neq m$ etc., however, they will not contaminate already existing Fourier harmonics, e.g., cc_{nn} etc. This process, we have discussed, is the most favorable for experimental measurements of GPDs by a number of reasons:

- it is a clean electromagnetic process which does not involve other unknown non-perturbative function and, thus, has no contamination from other unknown sources;
- the virtuality of the final state photon allows to disentangle the dependence of GPDs on both scaling variables and thus constrain the angular momentum sum rule;
- studies of the angular dependence of the recoiled nucleon and of the lepton pair are complementary and lead to a rich angular structure of the cross section that can be used for separation of diverse combinations of GPDs;
- variation of the relative magnitude of space- and timelike photon virtualities allows to access distributions of partons and anti-partons in the “exclusive” domain $\xi > |\eta|$.

- the higher one goes in skewness η , whose maximal value is limited by the magnitude of the momentum transfer to be within the region of applicability of QCD factorization $|\Delta^2| \ll p \cdot q$, the more surface in the exclusive domain ($|\eta| > |\xi|$) one measures in experiment. This diminishes the uncertainty coming from the inaccessible inclusive sector ($|\eta| < |\xi|$). The exclusive domain might saturate the spin sum rule (1) even for moderate η since the second moment required for it is not extremely sensitive to the large- ξ behavior of GPDs where the latter is known to decrease according to the quark-counting power law of conventional parton distributions.

Another interesting feature of this process is that the zero value of generalized Bjorken variable can be exactly attained when the incoming and outgoing photons have about the same absolute values of virtualities $Q^2 \simeq M_{\ell\bar{\ell}}^2$.

We have presently discussed the most favorable observables, namely, diverse lepton-spin and azimuthal asymmetries that are sensitive to the imaginary part of the Compton form factors and, thus, directly to GPDs. We have not discussed in full, however, phenomenological consequences of polarized targets, though, we have derived the complete set of formulas with explicit angular dependence which can be used to extract complimentary combinations of Compton form factors from experimental data. Longitudinal and transverse nucleon-spin asymmetries combined with the Fourier analysis will serve this purpose analogous to the lepton-spin asymmetries addressed presently. For the complete analysis along this line of exclusive electroproduction of a real photon see Ref. [9]. The process $eN \rightarrow e'N'\ell\bar{\ell}$ with both photons being virtual is unique due to the independence of skewness η from the generalized Bjorken variable ξ . Unfortunately, it suffers from very low cross sections, however, this drawback will be circumvented with future high-luminosity machines. The current analysis of available events from CLAS detector at Jefferson Laboratory is under way [32].

We would like to thank A.V. Radyushkin for useful discussions on the factorization issue and M. Diehl, M. Guidal, and M. Vanderhaeghen for discussions on phenomenological aspects of the paper. We thank the Department of Energy's Institute for Nuclear Theory at the University of Washington for its hospitality during the program "Generalized parton distributions and hard exclusive processes" and the Department of Energy for the partial support during the completion of this paper. The present work was supported by the US Department of Energy under contract DE-FG02-93ER40762.

A Light-cone vectors

The vectors defining the kinematics of the process can be used to construct a pair of the light-cone vectors n_μ and n_μ^* , such that $n^2 = n^{*2} = 0$ and $n \cdot n^* = 1$, as follows

$$\begin{aligned} n_\mu &= \frac{2\xi}{Q^2 \sqrt{1 + 4(\xi\delta)^2}} q_\mu - \frac{1 - \sqrt{1 + 4(\xi\delta)^2}}{2Q^2 \delta^2 \sqrt{1 + 4(\xi\delta)^2}} p_\mu, \\ n_\mu^* &= -\frac{\xi\delta^2}{\sqrt{1 + 4(\xi\delta)^2}} q_\mu + \frac{1 + \sqrt{1 + 4(\xi\delta)^2}}{4\sqrt{1 + 4(\xi\delta)^2}} p_\mu, \end{aligned} \quad (\text{A.1})$$

where $\delta^2 \equiv (M_N^2 - \Delta^2/4)/Q^2$. Throughout the paper we use the following decomposition of a given four-vector v_μ in its light-cone components

$$v_\mu = v_- n_\mu + v_+ n_\mu^* + v_\perp, \quad (\text{A.2})$$

so that a scalar product is written as $v \cdot u = v_+ u_- + v_- u_+ - \mathbf{v}_\perp \cdot \mathbf{u}_\perp$.

The light-cone decomposition of the momenta reads

$$\begin{aligned} p_\mu &= 2n_\mu^* + Q^2 \delta^2 n_\mu, \\ q_\mu &= -\frac{2\xi}{1 + \sqrt{1 + 4(\xi\delta)^2}} n_\mu^* - \frac{\xi Q^2 \delta^2}{1 - \sqrt{1 + 4(\xi\delta)^2}} n_\mu, \\ \Delta_\mu &= \frac{2\eta}{\sqrt{1 + 4(\xi\delta)^2}} n_\mu^* - \frac{\eta Q^2 \delta^2}{\sqrt{1 + 4(\xi\delta)^2}} n_\mu + \Delta_\mu^\perp. \end{aligned} \quad (\text{A.3})$$

Setting $\Delta_\perp = 0$ we get from the last equation the minimal value of Δ^2 , namely,

$$\Delta_{\min}^2 = \frac{Q^2}{2\xi^2} \left\{ 1 - \eta^2 + 4M_N^2 \xi^2 / Q^2 - \sqrt{(1 - \eta^2 + 4M_N^2 \xi^2 / Q^2)^2 + 16M_N^2 \xi^2 \eta^2 / Q^2} \right\}. \quad (\text{A.4})$$

B Results for polarized target

In the body of the paper we have given the results for the unpolarized nucleon target only. In the subsequent two appendices we fill the gap left and extend them by including polarization. We parametrize the polarization vector of the nucleon by a polar and an azimuthal angles Θ and Φ , respectively. In the target rest frame TRF-I it has the form (see Fig. 2)

$$S = (0, \sin \Theta \cos \Phi, \sin \Theta \sin \Phi, \cos \Theta). \quad (\text{B.1})$$

Introduction of the transverse polarization results into addition of an extra integration variable in the phase space given by Eqs. (3) and (6),

$$d\text{LIPS}_4 \rightarrow \frac{d\Phi}{2\pi} \times d\text{LIPS}_4. \quad (\text{B.2})$$

The Fourier coefficients $\text{ab}_{nm}^i = (\text{cc}_{nm}^i, \text{cs}_{nm}^i, \text{sc}_{nm}^i, \text{ss}_{nm}^i)$ depend on the nucleon polarization vector (B.1) and admit the decomposition

$$\text{ab}_{nm}^i = \text{ab}_{nm,\text{unp}}^i + \cos \Theta \text{ab}_{nm,\text{LP}}^i + \sin \Theta \text{ab}_{nm,\text{TP}}^i(\Phi). \quad (\text{B.3})$$

B.1 Squared VCS amplitude

The general structure of products of Compton form factors reads

$$\frac{1}{4} \mathcal{V} \mathcal{V}^\dagger \equiv \mathcal{C}_{\mathcal{V}\mathcal{V},\text{unp}}^{\text{VCS}} + \mathcal{C}_{\mathcal{V}\mathcal{V},\text{LP}}^{\text{VCS}} \cos \Theta + i \sqrt{-\frac{\Delta^2}{4M^2}} \sqrt{1 - \frac{\Delta_{\text{min}}^2}{\Delta^2}} \sqrt{\frac{1+\eta}{1-\eta}} \mathcal{C}_{\mathcal{V}\mathcal{V},\text{TP}}^{\text{VCS}} \sin(\Phi - \phi) \sin \Theta, \quad (\text{B.4})$$

$$\frac{1}{4} \mathcal{V} \mathcal{A}^\dagger \equiv \mathcal{C}_{\mathcal{V}\mathcal{A},\text{unp}}^{\text{VCS}} + \mathcal{C}_{\mathcal{V}\mathcal{A},\text{LP}}^{\text{VCS}} \cos \Theta + \sqrt{-\frac{\Delta^2}{4M^2}} \sqrt{1 - \frac{\Delta_{\text{min}}^2}{\Delta^2}} \sqrt{\frac{1+\eta}{1-\eta}} \mathcal{C}_{\mathcal{V}\mathcal{A},\text{TP}}^{\text{VCS}} \cos(\Phi - \phi) \sin \Theta, \quad (\text{B.5})$$

with \mathcal{A}^\dagger product having the decomposition similar to Eq. (B.4). Here the polar Θ and azimuthal Φ angles parametrize the nucleon polarization vector S according to Eq. (B.1). The nonvanishing \mathcal{C} -coefficients in the squared VCS amplitude, defined in Eq. (B.4-B.5) read for the polarized nucleon target

$$\mathcal{C}_{\mathcal{V}\mathcal{A},\text{LP}}^{\text{VCS}}(\mathcal{F}, \mathcal{F}^*) = (1 - \eta^2) \mathcal{H} \tilde{\mathcal{H}}^* - \eta^2 (\mathcal{H} \tilde{\mathcal{E}}^* + \mathcal{E} \tilde{\mathcal{H}}^*) + \eta \left(\frac{\Delta^2}{4M^2} + \frac{\eta^2}{1 - \eta} \right) \mathcal{E} \tilde{\mathcal{E}}^*, \quad (\text{B.6})$$

$$\mathcal{C}_{\mathcal{V}\mathcal{V},\text{TP}}^{\text{VCS}}(\mathcal{F}, \mathcal{F}^*) = (1 - \eta) (\mathcal{H} \mathcal{E}^* - \mathcal{E} \mathcal{H}^*), \quad (\text{B.7})$$

$$\mathcal{C}_{\mathcal{A}\mathcal{A},\text{TP}}^{\text{VCS}}(\mathcal{F}, \mathcal{F}^*) = (1 - \eta) \eta (\tilde{\mathcal{H}} \tilde{\mathcal{E}}^* - \tilde{\mathcal{E}} \tilde{\mathcal{H}}^*), \quad (\text{B.8})$$

$$\mathcal{C}_{\mathcal{V}\mathcal{A},\text{TP}}^{\text{VCS}}(\mathcal{F}, \mathcal{F}^*) = -(1 - \eta) (\eta \mathcal{H} \tilde{\mathcal{E}}^* + \mathcal{E} \tilde{\mathcal{H}}^*) + \eta^2 \mathcal{E} \tilde{\mathcal{E}}^*. \quad (\text{B.9})$$

We note that with this definitions, we have the following correspondence with those given in Ref. [9] for polarized target in the DVCS limit $\eta = -\xi$

$$\begin{aligned} \mathcal{C}_{\text{LP}}^{\text{DVCS}}(\mathcal{F}, \mathcal{F}^*) &\stackrel{\text{DVCS}}{=} \mathcal{C}_{\mathcal{V}\mathcal{A},\text{LP}}^{\text{VCS}}(\mathcal{F}, \mathcal{F}^*) + \mathcal{C}_{\mathcal{V}\mathcal{A},\text{LP}}^{\text{VCS}}(\mathcal{F}^*, \mathcal{F}), \\ \mathcal{C}_{\text{TP}+}^{\text{DVCS}}(\mathcal{F}, \mathcal{F}^*) &\stackrel{\text{DVCS}}{=} \mathcal{C}_{\mathcal{V}\mathcal{A},\text{TP}}^{\text{VCS}}(\mathcal{F}, \mathcal{F}^*) + \mathcal{C}_{\mathcal{V}\mathcal{A},\text{TP}}^{\text{VCS}}(\mathcal{F}^*, \mathcal{F}), \\ \mathcal{C}_{\text{TP}-}^{\text{DVCS}}(\mathcal{F}, \mathcal{F}^*) &\stackrel{\text{DVCS}}{=} \mathcal{C}_{\mathcal{V}\mathcal{V},\text{TP}}^{\text{VCS}}(\mathcal{F}, \mathcal{F}^*) + \mathcal{C}_{\mathcal{A}\mathcal{A},\text{TP}}^{\text{VCS}}(\mathcal{F}, \mathcal{F}^*). \end{aligned} \quad (\text{B.10})$$

The remaining Fourier coefficients read for longitudinally polarized target

$$\begin{aligned} \text{cc}_{00,\text{LP}}^{\text{VCS}} &= 2\lambda(2 - y)y(2 - 2\tilde{y} + \tilde{y}^2) \left\{ \mathcal{C}_{\mathcal{V}\mathcal{A},\text{LP}}^{\text{VCS}}(\mathcal{F}, \mathcal{F}^*) + \mathcal{C}_{\mathcal{V}\mathcal{A},\text{LP}}^{\text{VCS}}(\mathcal{F}^*, \mathcal{F}) \right\}, \\ \text{cc}_{11,\text{LP}}^{\text{VCS}} &= \lambda \frac{4\sigma}{\xi} y(2 - \tilde{y}) \sqrt{(1 - y)(1 - \tilde{y})(\xi^2 - \eta^2)} \left\{ \mathcal{C}_{\mathcal{V}\mathcal{A},\text{LP}}^{\text{VCS}}(\mathcal{F}_L, \mathcal{F}^*) + \mathcal{C}_{\mathcal{V}\mathcal{A},\text{LP}}^{\text{VCS}}(\mathcal{F}_L^*, \mathcal{F}) \right\}, \end{aligned} \quad (\text{B.11})$$

and for transversely polarized target

$$\text{cc}_{00,\text{TP}}^{\text{VCS}} = \sqrt{-\frac{\Delta^2}{M^2}} \sqrt{1 - \frac{\Delta_{\text{min}}^2}{\Delta^2}} \sqrt{\frac{1+\eta}{1-\eta}}$$

$$\begin{aligned}
& \times \left\{ \lambda \cos(\Phi - \phi) (2 - y) y (2 - 2\tilde{y} + \tilde{y}^2) \left\{ \mathcal{C}_{\mathcal{V}\mathcal{A},\text{TP}}^{\text{VCS}}(\mathcal{F}, \mathcal{F}^*) + \mathcal{C}_{\mathcal{V}\mathcal{A},\text{TP}}^{\text{VCS}}(\mathcal{F}^*, \mathcal{F}) \right\} \right. \\
& \quad + i \sin(\Phi - \phi) (2 - 2y + y^2) (2 - 2\tilde{y} + \tilde{y}^2) \left\{ \mathcal{C}_{\mathcal{V}\mathcal{V},\text{TP}}^{\text{VCS}}(\mathcal{F}, \mathcal{F}^*) + \mathcal{C}_{\mathcal{A}\mathcal{A},\text{TP}}^{\text{VCS}}(\mathcal{F}, \mathcal{F}^*) \right\} \\
& \quad \left. + 8i \sin(\Phi - \phi) (1 - y) (1 - \tilde{y}) \frac{\xi^2 - \eta^2}{\xi^2} \mathcal{C}_{\mathcal{V}\mathcal{V},\text{TP}}^{\text{VCS}}(\mathcal{F}_L, \mathcal{F}_L^*) \right\}, \tag{B.12}
\end{aligned}$$

$$\begin{aligned}
\text{cc}_{11,\text{TP}}^{\text{VCS}} &= \sqrt{-\frac{\Delta^2}{M^2}} \sqrt{1 - \frac{\Delta_{\min}^2}{\Delta^2}} \sqrt{\frac{1 + \eta}{1 - \eta}} \frac{2\sigma}{\xi} \sqrt{(1 - y)(1 - \tilde{y})(\xi^2 - \eta^2)} \\
& \times \left\{ \lambda \cos(\Phi - \phi) y (2 - \tilde{y}) \left\{ \mathcal{C}_{\mathcal{V}\mathcal{A},\text{TP}}^{\text{VCS}}(\mathcal{F}_L, \mathcal{F}^*) + \mathcal{C}_{\mathcal{V}\mathcal{A},\text{TP}}^{\text{VCS}}(\mathcal{F}_L^*, \mathcal{F}) \right\} \right. \\
& \quad \left. + i \sin(\Phi - \phi) (2 - y) (2 - \tilde{y}) \left\{ \mathcal{C}_{\mathcal{V}\mathcal{V},\text{TP}}^{\text{VCS}}(\mathcal{F}_L, \mathcal{F}^*) + \mathcal{C}_{\mathcal{V}\mathcal{V},\text{TP}}^{\text{VCS}}(\mathcal{F}_L^*, \mathcal{F}) \right\} \right\}, \tag{B.13}
\end{aligned}$$

$$\begin{aligned}
\text{cc}_{22,\text{TP}}^{\text{VCS}} &= \sqrt{-\frac{\Delta^2}{M^2}} \sqrt{1 - \frac{\Delta_{\min}^2}{\Delta^2}} \sqrt{\frac{1 + \eta}{1 - \eta}} \\
& \times 4i \sin(\Phi - \phi) (1 - y) (1 - \tilde{y}) \left\{ \mathcal{C}_{\mathcal{V}\mathcal{V},\text{TP}}^{\text{VCS}}(\mathcal{F}, \mathcal{F}^*) - \mathcal{C}_{\mathcal{A}\mathcal{A},\text{TP}}^{\text{VCS}}(\mathcal{F}, \mathcal{F}^*) \right\}, \tag{B.14}
\end{aligned}$$

where according to the general twist-two relation (105)

$$\text{ss}_{11,\text{LP/TP}}^{\text{VCS}} \simeq \text{cc}_{11,\text{LP/TP}}^{\text{VCS}}, \quad \text{ss}_{22,\text{TP}}^{\text{VCS}} \simeq \text{cc}_{22,\text{TP}}^{\text{VCS}}. \tag{B.15}$$

B.2 Interference term

Similarly to the previous appendix, we present here the results for the interference term on a polarized target.

$$\begin{aligned}
\begin{Bmatrix} \mathcal{S}_1 \\ \mathcal{S}_2 \end{Bmatrix}_{\mathcal{V}} &\equiv 4Q^2 \frac{(1 - \eta)\eta}{y\tilde{y}\xi} \left(\begin{Bmatrix} \tilde{y}K \\ y\tilde{K} \end{Bmatrix} \left[-\mathcal{C}_{\mathcal{V},\text{unp}}(\mathcal{F}) \begin{Bmatrix} \cos \phi \\ \cos \varphi_\ell \end{Bmatrix} - \cos \Theta i\mathcal{C}_{\mathcal{V},\text{LP}}(\mathcal{F}) \begin{Bmatrix} \sin \phi \\ \sin \varphi_\ell \end{Bmatrix} \right] \right. \\
& \quad \left. - \sin \Theta \begin{Bmatrix} \tilde{y}L \\ y\tilde{L} \end{Bmatrix} \left[i\mathcal{C}_{\mathcal{V},\text{TP}+}(\mathcal{F}) \begin{Bmatrix} \sin \phi \\ \sin \varphi_\ell \end{Bmatrix} \cos(\Phi - \phi) + i\mathcal{C}_{\mathcal{V},\text{TP}-}(\mathcal{F}) \begin{Bmatrix} \cos \phi \\ \cos \varphi_\ell \end{Bmatrix} \sin(\Phi - \phi) \right] \right), \tag{B.16}
\end{aligned}$$

$$\begin{aligned}
\begin{Bmatrix} \mathcal{R}_1 \\ \mathcal{R}_2 \end{Bmatrix}_{\mathcal{V}} &\equiv 4Q^2 \frac{(1 - \eta)\eta}{y\tilde{y}\xi} \left(\begin{Bmatrix} \tilde{y}K \\ y\tilde{K} \end{Bmatrix} \left[i\mathcal{C}_{\mathcal{V},\text{unp}}(\mathcal{F}) \begin{Bmatrix} \sin \phi \\ \sin \varphi_\ell \end{Bmatrix} + \cos \Theta \mathcal{C}_{\mathcal{V},\text{LP}}(\mathcal{F}) \begin{Bmatrix} \cos \phi \\ \cos \varphi_\ell \end{Bmatrix} \right] \right. \\
& \quad \left. + \sin \Theta \begin{Bmatrix} \tilde{y}L \\ y\tilde{L} \end{Bmatrix} \left[\mathcal{C}_{\mathcal{V},\text{TP}+}(\mathcal{F}) \begin{Bmatrix} \cos \phi \\ \cos \varphi_\ell \end{Bmatrix} \cos(\Phi - \phi) - \mathcal{C}_{\mathcal{V},\text{TP}-}(\mathcal{F}) \begin{Bmatrix} \sin \phi \\ \sin \varphi_\ell \end{Bmatrix} \sin(\Phi - \phi) \right] \right), \tag{B.17}
\end{aligned}$$

$$\begin{aligned}
\begin{Bmatrix} \mathcal{S}_1 \\ \mathcal{S}_2 \end{Bmatrix}_{\mathcal{A}} &\equiv 4Q^2 \frac{(1 - \eta)\eta}{y\tilde{y}\xi} \left(\begin{Bmatrix} \tilde{y}K \\ y\tilde{K} \end{Bmatrix} \left[-i\mathcal{C}_{\mathcal{A},\text{unp}}(\mathcal{F}) \begin{Bmatrix} \sin \phi \\ \sin \varphi_\ell \end{Bmatrix} - \cos \Theta \mathcal{C}_{\mathcal{A},\text{LP}}(\mathcal{F}) \begin{Bmatrix} \cos \phi \\ \cos \varphi_\ell \end{Bmatrix} \right] \right. \\
& \quad \left. - \sin \Theta \begin{Bmatrix} \tilde{y}L \\ y\tilde{L} \end{Bmatrix} \left[\mathcal{C}_{\mathcal{A},\text{TP}+}(\mathcal{F}) \begin{Bmatrix} \cos \phi \\ \cos \varphi_\ell \end{Bmatrix} \cos(\Phi - \phi) - \mathcal{C}_{\mathcal{A},\text{TP}-}(\mathcal{F}) \begin{Bmatrix} \sin \phi \\ \sin \varphi_\ell \end{Bmatrix} \sin(\Phi - \phi) \right] \right), \tag{B.18}
\end{aligned}$$

$$\begin{aligned} \left\{ \begin{matrix} \mathcal{R}_1 \\ \mathcal{R}_2 \end{matrix} \right\} \mathcal{A} \equiv & 4Q^2 \frac{(1-\eta)\eta}{y\tilde{y}\xi} \left(\left\{ \begin{matrix} \tilde{y}K \\ y\tilde{K} \end{matrix} \right\} \left[\mathcal{C}_{\mathcal{A},\text{unp}}(\mathcal{F}) \begin{Bmatrix} \cos \phi \\ \cos \varphi_\ell \end{Bmatrix} + \cos \Theta i\mathcal{C}_{\mathcal{A},\text{LP}}(\mathcal{F}) \begin{Bmatrix} \sin \phi \\ \sin \varphi_\ell \end{Bmatrix} \right] \right. \\ & \left. + \sin \Theta \left\{ \begin{matrix} \tilde{y}L \\ y\tilde{L} \end{matrix} \right\} \left[i\mathcal{C}_{\mathcal{A},\text{TP}+}(\mathcal{F}) \begin{Bmatrix} \sin \phi \\ \sin \varphi_\ell \end{Bmatrix} \cos(\Phi - \phi) + i\mathcal{C}_{\mathcal{A},\text{TP}-}(\mathcal{F}) \begin{Bmatrix} \cos \phi \\ \cos \varphi_\ell \end{Bmatrix} \sin(\Phi - \phi) \right] \right) , \end{aligned} \quad (\text{B.19})$$

where we used in analogy to the definitions (37) the shorthand notation

$$\left\{ \begin{matrix} L \\ \tilde{L} \end{matrix} \right\} \approx -\frac{1}{2\eta} \sqrt{\frac{\xi M^2}{Q^2}} \left\{ \begin{matrix} \sqrt{(1-y)(\xi-\eta)} \\ \sqrt{(1-\tilde{y})(\xi+\eta)} \end{matrix} \right\} \quad (\text{B.20})$$

For the longitudinally polarized nucleon, we get the following combinations of the electromagnetic and Compton form factors:

$$\mathcal{C}_{\mathcal{V},\text{LP}} = -\eta(F_1 + F_2) \left(\mathcal{H} - \frac{\eta}{1-\eta} \mathcal{E} \right), \quad \mathcal{C}_{\mathcal{A},\text{LP}} = F_1 \tilde{\mathcal{H}} - \eta \left(\frac{\eta}{1-\eta} F_1 - \frac{\Delta^2}{4M_N^2} F_2 \right) \tilde{\mathcal{E}}, \quad (\text{B.21})$$

while for the transversal case we have four more combinations

$$\mathcal{C}_{\mathcal{V},\text{TP}+} = \frac{2\eta}{1-\eta} (F_1 + F_2) \left\{ \eta \left(\mathcal{H} - \frac{\eta}{1-\eta} \mathcal{E} \right) - \frac{\Delta^2}{4M_N^2} \mathcal{E} \right\}, \quad (\text{B.22})$$

$$\mathcal{C}_{\mathcal{A},\text{TP}+} = -\frac{2}{1-\eta} \left\{ \eta^2 F_1 \left(\tilde{\mathcal{H}} - \frac{\eta}{1-\eta} \tilde{\mathcal{E}} \right) - \frac{\Delta^2}{4M_N^2} \left((1-\eta^2) F_2 \tilde{\mathcal{H}} + \eta(F_1 - \eta F_2) \tilde{\mathcal{E}} \right) \right\}, \quad (\text{B.23})$$

$$\mathcal{C}_{\mathcal{V},\text{TP}-} = \frac{2}{1-\eta} \left\{ \eta^2 F_1 (\mathcal{H} + \mathcal{E}) - \frac{\Delta^2}{4M_N^2} \left((1-\eta^2) F_2 \mathcal{H} - (F_1 + \eta^2 F_2) \mathcal{E} \right) \right\}, \quad (\text{B.24})$$

$$\mathcal{C}_{\mathcal{A},\text{TP}-} = -\frac{2\eta^2}{1-\eta} (F_1 + F_2) \left\{ \tilde{\mathcal{H}} + \frac{\Delta^2}{4M_N^2} \tilde{\mathcal{E}} \right\}. \quad (\text{B.25})$$

First, we display the explicit form of the Fourier coefficient in the interference term with the second BH process for an unpolarized nucleon target, which we deduced by symmetry considerations in the main text. They are

$$\text{cc}_{01,\text{unp}}^2 = 8K(2-y)(1-\tilde{y})(2-\tilde{y}) \frac{\xi+\eta}{\eta} \Re \left\{ \mathcal{C}_{\mathcal{V},\text{unp}}(\mathcal{F}) - \mathcal{C}_{\mathcal{A},\text{unp}}(\mathcal{F}) - \frac{\xi-\eta}{\xi} \mathcal{C}_{\mathcal{V},\text{unp}}(\mathcal{F}_L) \right\}, \quad (\text{B.26})$$

$$\text{cs}_{01,\text{unp}}^2 = 8\lambda K y(1-\tilde{y})(2-\tilde{y}) \frac{\xi+\eta}{\eta} \Im \left\{ -\mathcal{C}_{\mathcal{V},\text{unp}}(\mathcal{F}) + \mathcal{C}_{\mathcal{A},\text{unp}}(\mathcal{F}) - \frac{\xi-\eta}{\xi} \mathcal{C}_{\mathcal{V},\text{unp}}(\mathcal{F}_L) \right\}, \quad (\text{B.27})$$

$$\begin{aligned} \text{cc}_{10,\text{unp}}^2 = & -8\tilde{K} \Re \left\{ (2-2y+y^2)(2-2\tilde{y}+\tilde{y}^2) \left(\frac{\xi}{\eta} \mathcal{C}_{\mathcal{V},\text{unp}}(\mathcal{F}) - \mathcal{C}_{\mathcal{A},\text{unp}}(\mathcal{F}) \right) \right. \\ & \left. -8(1-y)(1-\tilde{y}) \frac{\xi^2-\eta^2}{\eta\xi} \mathcal{C}_{\mathcal{V},\text{unp}}(\mathcal{F}_L) \right\}, \end{aligned} \quad (\text{B.28})$$

$$\text{cc}_{12,\text{unp}}^2 = -16\tilde{K}(1-y)(1-\tilde{y}) \frac{\xi-\eta}{\eta} \Re \left\{ \mathcal{C}_{\mathcal{V},\text{unp}}(\mathcal{F}) - \mathcal{C}_{\mathcal{A},\text{unp}}(\mathcal{F}) \right\}, \quad (\text{B.29})$$

$$\text{sc}_{10,\text{unp}}^2 = 8\lambda\tilde{K} y(2-y)(2-2\tilde{y}+\tilde{y}^2) \Im \left\{ \mathcal{C}_{\mathcal{V},\text{unp}}(\mathcal{F}) - \frac{\xi}{\eta} \mathcal{C}_{\mathcal{A},\text{unp}}(\mathcal{F}) \right\}, \quad (\text{B.30})$$

$$\text{cc}_{21,\text{unp}}^2 = 8K(2-y)(1-\tilde{y})(2-\tilde{y})\frac{\xi+\eta}{\eta}\Re\left\{\mathcal{C}_{\mathcal{V},\text{unp}}(\mathcal{F}) + \mathcal{C}_{\mathcal{A},\text{unp}}(\mathcal{F}) - \frac{\xi+\eta}{\xi}\mathcal{C}_{\mathcal{V},\text{unp}}(\mathcal{F}_L)\right\} \quad (\text{B.31})$$

$$\text{sc}_{21,\text{unp}}^2 = -8\lambda Ky(1-\tilde{y})(2-\tilde{y})\frac{\xi+\eta}{\eta}\Im\left\{\mathcal{C}_{\mathcal{V},\text{unp}}(\mathcal{F}) + \mathcal{C}_{\mathcal{A},\text{unp}}(\mathcal{F}) + \frac{\xi+\eta}{\xi}\mathcal{C}_{\mathcal{V},\text{unp}}(\mathcal{F}_L)\right\} \quad (\text{B.32})$$

$$\text{cc}_{32,\text{unp}}^2 = -16\tilde{K}(1-y)(1-\tilde{y})\frac{\xi+\eta}{\eta}\Re\left\{\mathcal{C}_{\mathcal{V},\text{unp}}(\mathcal{F}) + \mathcal{C}_{\mathcal{A},\text{unp}}(\mathcal{F})\right\}. \quad (\text{B.33})$$

Next we consider the Fourier coefficients for a polarized target. From the results (B.16)-(B.19) we immediately read off several relations which allows us to obtain the expression for the Fourier coefficients making use of simple substitution rules in the unpolarized case (119)-(126) and (B.26)-(B.33):

$$\begin{aligned} \{\text{cc}_{01}, \text{cc}_{10}, \text{cc}_{21}\}_{\text{LP}}^{\text{INT}} &= \{\text{cs}_{01}, \text{sc}_{10}, \text{sc}_{21}\}_{\text{unp}}^{\text{INT}} \Big|_{\Im\mathcal{C}_{\text{unp}} \rightarrow \Re\mathcal{C}_{\text{LP}}}, \\ \{\text{cs}_{01}, \text{sc}_{10}, \text{cs}_{12}, \text{sc}_{21}, \text{sc}_{32}\}_{\text{LP}}^{\text{INT}} &= \{\text{cc}_{01}, \text{cc}_{10}, \text{cc}_{12}, \text{cc}_{21}, \text{cc}_{32}\}_{\text{unp}}^{\text{INT}} \Big|_{\Re\mathcal{C}_{\text{unp}} \rightarrow \Im\mathcal{C}_{\text{LP}}}. \end{aligned} \quad (\text{B.34})$$

In the case of a transversely polarized target we have as before an additional decomposition in $\cos(\Phi - \phi)$ and $\sin(\Phi - \phi)$ and should replace K (\tilde{K}) by L (\tilde{L})

$$\begin{aligned} \{\text{cc}_{01}, \text{cc}_{10}, \text{cc}_{21}\}_{\text{TP}+}^{\text{INT}} &= \cos(\Phi - \phi) \{\text{cs}_{01}, \text{sc}_{10}, \text{sc}_{21}\}_{\text{unp}}^{\text{INT}} \Big|_{\substack{\Im\mathcal{C}_{\text{unp}} \rightarrow \Re\mathcal{C}_{\text{TP}+} \\ K \rightarrow L, \tilde{K} \rightarrow \tilde{L}}}, \\ \{\text{cs}_{01}, \text{sc}_{10}, \text{sc}_{21}\}_{\text{TP}-}^{\text{INT}} &= \sin(\Phi - \phi) \{\text{cs}_{01}, \text{sc}_{10}, \text{sc}_{21}\}_{\text{unp}}^{\text{INT}} \Big|_{\substack{\Im\mathcal{C}_{\text{unp}} \rightarrow -\Re\mathcal{C}_{\text{TP}-} \\ K \rightarrow L, \tilde{K} \rightarrow \tilde{L}}}, \\ \{\text{cs}_{01}, \text{sc}_{10}, \text{cs}_{12}, \text{sc}_{21}, \text{sc}_{32}\}_{\text{TP}+}^{\text{INT}} &= \cos(\Phi - \phi) \{\text{cc}_{01}, \text{cc}_{10}, \text{cc}_{12}, \text{cc}_{21}, \text{cc}_{32}\}_{\text{unp}}^{\text{INT}} \Big|_{\substack{\Re\mathcal{C}_{\text{unp}} \rightarrow \Im\mathcal{C}_{\text{TP}+} \\ K \rightarrow L, \tilde{K} \rightarrow \tilde{L}}}, \\ \{\text{cc}_{01}, \text{cc}_{10}, \text{cc}_{12}, \text{cc}_{23}, \text{cc}_{32}\}_{\text{TP}-}^{\text{INT}} &= \sin(\Phi - \phi) \{\text{cc}_{01}, \text{cc}_{10}, \text{cc}_{12}, \text{cc}_{23}, \text{cc}_{32}\}_{\text{unp}}^{\text{INT}} \Big|_{\substack{\Re\mathcal{C}_{\text{unp}} \rightarrow \Im\mathcal{C}_{\text{TP}-} \\ K \rightarrow L, \tilde{K} \rightarrow \tilde{L}}}. \end{aligned} \quad (\text{B.35})$$

Applying the relation (113), the remaining nonvanishing Fourier coefficients, i.e., $\text{ss}_{21}^{\text{INT}}$, $\text{sc}_{12}^{\text{INT}}$, $\text{cs}_{21}^{\text{INT}}$, $\text{cs}_{23}^{\text{INT}}$ for LP and TP+ as well as $\text{ss}_{12}^{\text{INT}}$, $\text{ss}_{21}^{\text{INT}}$, $\text{ss}_{23}^{\text{INT}}$ and $\text{cs}_{21}^{\text{INT}}$ for TP- are easily established.

References

- [1] D. Müller, D. Robaschik, B. Geyer, F.-M. Dittes, J. Horejsi, Fortschr. Phys. 42 (1994) 101.
- [2] X. Ji, Phys. Rev. D 55 (1997) 7114.
- [3] A.V. Radyushkin, Phys. Rev. D 56 (1997) 5524.
- [4] A.V. Belitsky, *Renormalons in exclusive meson electroproduction*, hep-ph/0307256.
- [5] X. Ji, *Viewing the proton through “color” filters*, hep-ph/0304037.
- [6] X. Ji, Phys. Rev. Lett. 78 (1997) 610.

- [7] M. Diehl, T. Gousset, B. Pire, J.P. Ralston, Phys. Lett. B 411 (1997) 193.
- [8] A.V. Belitsky, D. Müller, L. Niedermeier, A. Schäfer, Nucl. Phys. B 593 (2001) 289.
- [9] A.V. Belitsky, D. Müller, A. Kirchner, Nucl. Phys. B 629 (2002) 323.
- [10] E.R. Berger, M. Diehl, B. Pire, Eur. Phys. J. C 23 (2002) 675.
- [11] A.V. Belitsky, D. Müller, Phys. Rev. Lett. 90 (2003) 022001.
- [12] M. Guidal, M. Vanderhaeghen, Phys. Rev. Lett. 90 (2003) 012001.
- [13] J.C. Collins, A. Freund, Phys. Rev. D 59 (1999) 074009.
- [14] M.A. Shifman, A.I. Vainshtein, V.I. Zakharov, Nucl. Phys. B 147 (1979) 347.
- [15] A.V. Radyushkin, Phys. Lett. B 449 (1999) 81.
- [16] A.V. Efremov, A.V. Radyushkin, Theor. Math. Phys. 44 (1981) 774.
- [17] J.M.F. Labastida, G. Sterman, Nucl. Phys. B 254 (1985) 425.
- [18] J.C. Collins, D.E. Soper, G. Sterman, *Factorization of hard process in QCD*, in *Perturbative QCD*, ed. A.H. Mueller, World Scientific (Singapore, 1989) p. 1.
- [19] A.V. Belitsky, X. Ji, F. Yuan, Nucl. Phys. B 656 (2003) 165.
- [20] A.V. Belitsky, D. Müller, Nucl. Phys. B 589 (2000) 611.
- [21] I.V. Anikin, B. Pire, O.V. Teryaev, Phys. Rev. D 62 (2000) 071501.
- [22] M. Penttinen, M.V. Polyakov, A.G. Shuvaev, M. Strikman, Phys. Lett. B 491 (2000) 96.
- [23] A.V. Radyushkin, C. Weiss, Phys. Rev. D 63 (2001) 114012.
- [24] X. Ji, J. Osborne, Phys. Rev. D 58 (1998) 094018.
- [25] A.V. Belitsky, D. Müller, Phys. Lett. B 417 (1998) 129.
- [26] L. Mankiewicz, G. Piller, E. Stein, M. Vanttinen, T. Weigl, Phys. Lett. B 425 (1998) 186.
- [27] P. Hoodbhoy, X. Ji, Phys. Rev. D 58 (1998) 054006.
- [28] A.V. Belitsky, D. Müller, Phys. Lett. B 486 (2000) 369.
- [29] M.V. Polyakov, C. Weiss, Phys. Rev. D 60 (1999) 114017.

- [30] P. Schweitzer, S. Boffi, M. Radici, Phys. Rev. D 66 (2002) 114004.
- [31] K. Goeke, M.V. Polyakov, M. Vanderhaeghen, Prog. Part. Nucl. Phys. 47 (2001) 401.
- [32] M. Garçon, talk at *User group symposium and annual meeting: A celebration of JLab physics*,
<http://www.jlab.org/intralab/calendar/archive03/ugm/talks/garcon.pdf>.